Handlebody Plesiohedra Unchained:
Topologically Interlocked Cell-Transitive 3-Honeycombs

Matthew Ebert[a], Doyeon Kim[b], Ergun Akleman[b,c], Vinayak Krishnamurthy[a,c]

[a] *J. Mike Walker '66 Department of Mechanical Engineering, Texas A&M University*
[b] *Department of Visualization, Texas A&M University*
[c] *Department of Computer Science & Engineering (By Affiliation), Texas A&M University*

Abstract

We present an approach for systematic design of generalized Plesiohedra, a new type of 3D space-filling shapes that can even include unchained handlebodies. We call these handlebody plesiohedra unchained, since they are **topologically interlocked**, i.e., they can be assembled and disassembled without breaking any of the solids apart and they can keep in place with a set of boundary constraints. These space-filling shapes (i.e. congruent prototiles) are obtained from the Voronoi decomposition of symmetric Delone (Delaunay) point sets. To create this new class of shapes, we generalize the design space of classical Plesiohedra by introducing two novel geometric steps: (a) extension of point sites to piecewise linear approximations of higher-dimensional geometries and (b) extension of symmetries to 3D crystallographic symmetries. We show how these specific collections of higher-dimensional geometries can admit the symmetric Delone property. A Voronoi partitioning of 3D space using these specific collections of higher-dimensional shapes as Voronoi sites naturally results in congruent prototiles. This generalizes the idea of classical Plesiohedra by allowing for piecewise linear approximation of curved edges and faces, non-convex boundaries, and even handlebodies with positive genus boundaries to provide truly volumetric material systems in contrast to traditional planar or shell-like systems. To demonstrate existence of these solid shapes, we produced a large set of unchained congruent space-filling handlebodies as proofs of concept. For this, we focused our investigation using isometries of some space-filling polyhedra, such as a cube and a truncated octahedron with circles, and curve complexes as Voronoi sites. These results point to a rich and vast parametric design space of unchained handlebody plesiohedra making them an excellent representations for engineering applications such as topologically interlocked architectured materials.

1. Introduction

In this work, we present a computational methodology for generating volumetric **topologically interlocked** tessellations, i.e. decomposition of 3D-space with topologically interlocked congruent solid handlebodies (Figure 1). In geometric topology, a solid handlebody is defined as an orientable 3-manifold-with-boundary containing pairwise disjoint, properly embedded 2-discs such that the manifold resulting from cutting along the discs is a 3-ball [1]. An important property of solid handlebodies is that their boundary can be a surface of any genus, and the genus of a handlebody is the genus of its boundary surface.

There exists a significant amount of work on space-filling shapes, i.e., the shape that can be repeatably tiled to tessellate a given space in a watertight manner [2]. Most of the systematic methods are based on plesiohedra, space filling shapes that are naturally emerging from Voronoi tessellations induced by a special class of point arrangements known as symmetric Delone[1] (Delaunay) sets. Most commonly known spece-filling 3D polyhedra, such as cubes, truncated octahedra, hexagonal prisms, and rhombic dodecahedrons, can be viewed as special cases of plesiohedra that are generated through Voronoi tessellations of symmetrically arranged point sets.

While the Voronoi-based plesiohedral approach is elegant, it suffers from a significant limitation in that it assumes the Voronoi sites to be points. Point sets, when used as Voronoi sites, can only produce convex polyhedra with planar faces and straight edges. **To discover new types of plesiohedral shapes beyond planar convex shapes, new approaches are needed.** In this paper, we present such an approach for the systematic design of more generalized plesiohedra (see Figure 1). Our approach is a generalization of the classical plesiohedral approach in the sense that it allows us to produce arbitrary genus handlebodies as Voronoi sites (see Figure 2 for examples).

In this work, we are particularly interested in producing solid shapes with holes. However, we do not want to produce chained structures since chains are geometrically interlocked structures that cannot be disassembled or assembled [3]. Instead, we want each solid shape to be manufactured individually and assembled to form larger structures. Moreover, we want these assemblies to stay in place once the boundaries have been constrained. In other words, we want our structures to be **topologically interlocked** [3]. The reason we want to have holes and curved faces is to further improve the topological interlocking property so that the whole assembly can remain together without great effort using a few boundary constraints.

1.1. Application Context & Motivation

Space-filling shapes are important in many applications of science, engineering, and architecture [2, 4, 5]. A space-filling

Email addresses: `ergun.akleman@gmail.com` (Ergun Akleman), `vinayak@tamu.edu` (Vinayak Krishnamurthy)

[1] *Delone* is a transliteration of Boris Delaunay's last name that was used in later publications. We have used this version when referring to symmetric Delone sets, in keeping with the prevalent tradition in the mathematics literature.

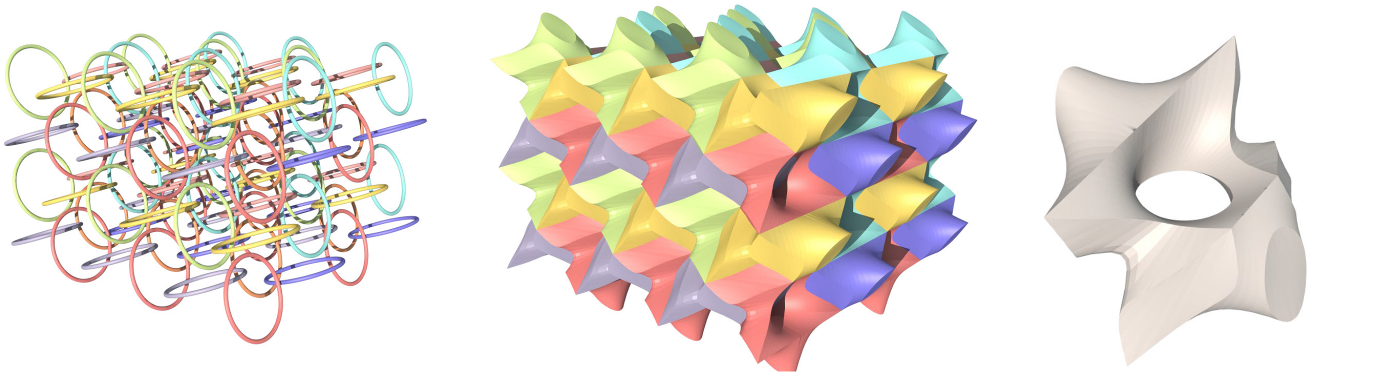

(a) A 3D assembly of un-linked circles that are closed under a symmetry operation induced by cube isometries.

(b) A Cell-Transitive 3-Honeycomb as a Voronoi decomposition of the space using circles shown in Figure 1a.

(c) A genus-1 handlebody shape with curved edges and faces that can fill 3D space with no gap.

Figure 1: This Figure shows how genus-1 handlebody plesiohedral shapes are obtained. The curved edges and faces are approximated by planar regions that are resulting from union of convex Voronoi polyhedra that are obtained by using points that approximate high-dimensional shapes.

shape is one that can be tiled without any gaps to generate a tessellation — a *cell-transitive* honeycomb — of a given space. In general, the idea of honeycombs has often been used to design a variety of 2D as well as 3D foam structures [6, 7, 8, 9], by leveraging Voronoi tessellations. These are primarily *inverse design* methods that employ some form of stochastic (or other) sampling strategy, typically in conjunction with physics-based structural evaluation, to generate an optimal structure for some specific application. As a result, the geometric relationship between the parameter space and the resulting shapes is not explicitly available to the designer.

Interestingly, even cell-transitive honeycombs have been widely used (albeit without reference to the concept) for applications such as the design of lattice-based materials systems [10], interlocking materials systems [11, 12, 13, 14], osteomorphic materials systems [15] and auxetic materials [16]. An advantage of the cell-transitive property is that the designer has complete control over the parameter space that generates these structures. In other words, the geometric representation of these structures can be tailored for both forward and inverse design. However, current work on cell-transitive honeycombs is, by and large, limited to 2D or 2.5D spatial domains, that is, domains where a planar tessellation is extruded (2D) or varies locally within a thin-shell-like volume(2.5D). An exception is the work of Wang and Rai that demonstrates the generative design of 3D foams based on Fourier functions [17]. However, even this approach is suitable mainly for inverse design as the input parameters (driving the Fourier functions) are not intuitive for manual specification and control. Some recent works have also used topology optimization to create complex and variable foams for arbitrary structures [18]

Our work aims to develop a geometric representation for the design of space-filling 3D shapes that offers an intuitive parameterization for the systematic forward design of such shapes while simultaneously enabling effective inverse design possibilities in the future. To achieve this aim, our methodology combines three geometric concepts, namely Voronoi tessellation to ensure the space-filling property, the use of higher-dimensional geometries (lines, curves, curve networks, etc.) as Voronoi sites to expose a large design space, and the spatial arrangement of these sites using a carefully selected subset of 3D crystallographic symmetries.

1.2. Problem & Knowledge Gaps

In geometry, a *honeycomb* is a tessellation of space, i.e., a close packing of simpler shapes without leaving any gaps [19]. Honeycombs can be defined for any Euclidean space (called an n-Honeycomb for $\mathbb{R}^n$) and even for non-Euclidean (e.g., hyperbolic) spaces [20]. Consider a 3-Honeycomb (i.e., a tessellation of $\mathbb{R}^3$) such that all the shapes in this honeycomb are congruent. Such a 3-Honeycomb is defined as a cell-transitive (or isochoric) [21] honeycomb. The *unit* shape that generates a cell-transitive honeycomb is a space-filling shape or *prototiles* [2].

While cell-transitive honeycombs have been extensively studied in 2D Euclidean space [22, 23], very little is understood regarding cell-transitive 3-honeycombs. The specific problem of generating plesiohedra (which are a special class of stereohedra specifically generated through Voronoi tessellations) is equivalent to the problem of generating arrangements of points (Voronoi sites) according to some space groups (or symmetry groups in a given Euclidean space). As such, there is no dearth of literature that categorizes and characterizes spatial symmetry groups and the resulting tessellations [24, 25]. In fact, Schmitt [25] offers a comprehensive classification of space groups in relation to plesiohedra. Despite such extensive literature on the subject, three fundamental gaps make it difficult to translate existing theories of spatial symmetries into effective methodologies for design applications.

Space-filling Polyhedra

The work on space filling structures in 3D is generally focused on polyhedral shapes, and the identification of new space filling polyhedra has been an art that requires mathematical creativity and ingenuity [26]. In fact, currently known stereohedra (the superset of plesiohedra) are all primarily convex polyhedra. Goldberg exhaustively cataloged many known space-filling polyhedra with a series of papers from 1972 to 1982 such as [27, 28, 29, 30, 31, 32, 33, 34]. We now know that there are eight space-filling convex polyhedra and five of them have regular faces, namely the triangular prism, hexagonal prism, cube,

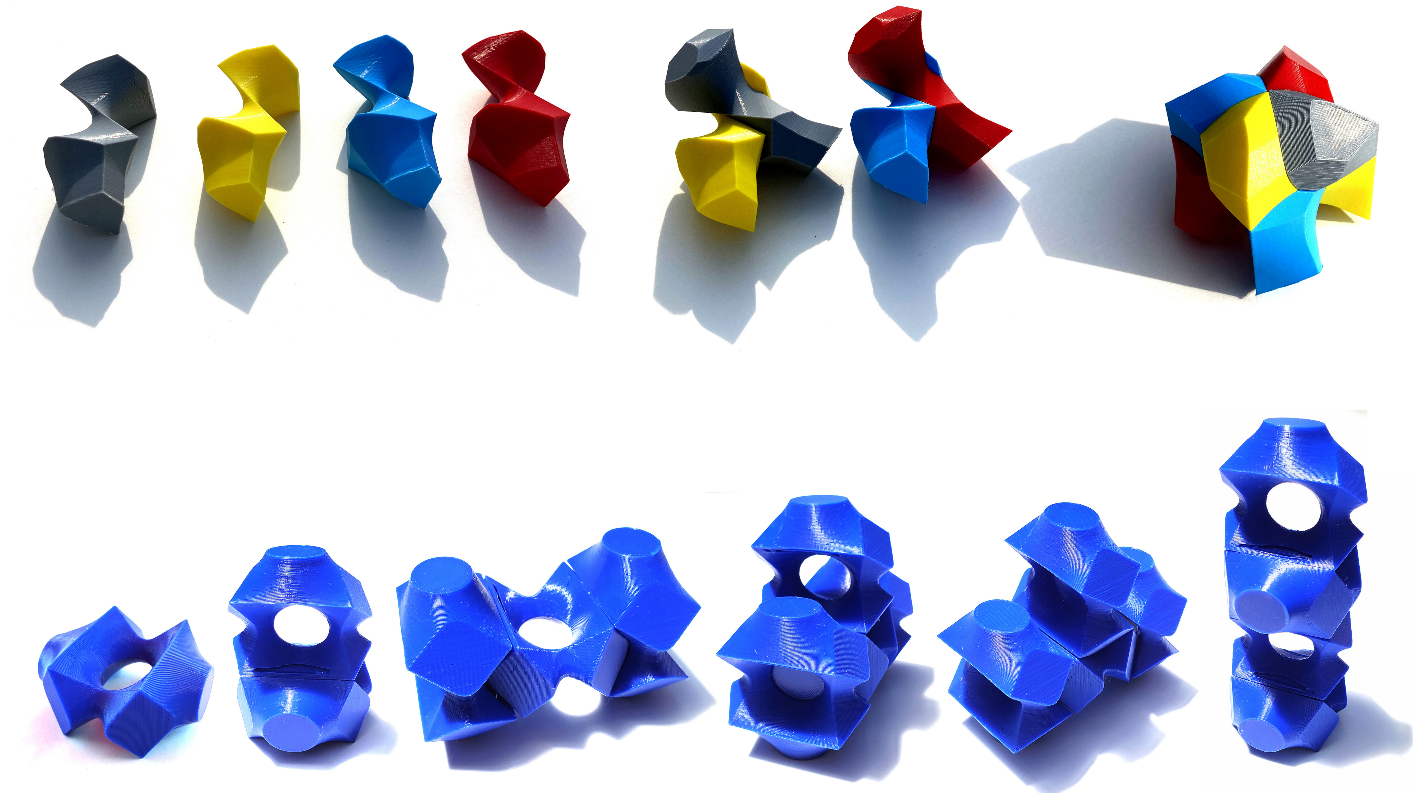

Figure 2: Two examples of 3D printed plesiohedra as a single piece and an assembly of the shapes. These particular plesiohedral shapes are obtained by using lines (top) or circles(bottom) as Voronoi sites closed under space symmetries.

truncated octahedron [35, 36], and *gyrobifastigium* [37, 38]. Five of these eight space-filling shapes are "primary" parallelohedra [39], namely cube, hexagonal prism, rhombic dodecahedron, elongated dodecahedron, and truncated octahedron. For the first time, we show in this paper that the design space of plesiohedra is much larger than what has been reported and includes arbitrarily complex, non-convex, and positive genus prototiles.

Patterns in Architectural and Engineering Design

The last two decades have seen significant work in computer graphics for pattern generation for artistic [40], architectural [41], and engineering applications. A large category of work in this domain seeks to generate patterns on 2-manifolds (surfaces). For instance, Akleman's work on symmetric tilings [12] and surface patterning based on weaves [42] are examples that utilize mesh topology operations to generalize weave generation on regular surface meshes. Two prominent recent works are free-form honeycomb structures [43] and polyhedral patterns [44], both of which show interesting methods to map a given tiling with the differential geometric properties of the underlying surface. Most recently, work by Meekes et al. [45] generalized de Bruijn's multigrid method to discrete surfaces to generate several periodic and aperiodic tilings on surfaces. Another class of methods focuses primarily on regular and semi-regular cellular structures for a wide variety of metamaterial design problems. Here, two prominent examples are structured sheet materials [46] and star-shaped metamaterials [10] that investigate the mechanical properties of planar cellular patterns. As such, all these methods are focused on extending planar patterns to arbitrary 2-manifolds embedded in 3D space.

There is significant work in the design of interlocking structures with applications in both architectural and metamaterial design (see [3] for a review). Séquin shows a clever way to assemble and disassemble positive-genus congruent shapes by fabricating two or more separate pieces that can be interlocked [47]. Decomposing single genus-1 tiles into genus-0 pieces helped assemble and disassemble the linked structures. Recent seminal work by Wang et al. [48] presented a method for optimal design of topologically interlocking structures based on a comprehensive physics-based model. Several recent works demonstrate 2.5D tessellations for a variety of topologically and geometrically interlocking tiles. However, these methods primarily use symmetries in 2D Euclidean space and, as a result, are restricted to arrangements of prototiles either in the plane [11, 13] or on surfaces [14]. Although one can argue that planar arrangements could simply be stacked to create a volumetric tiling (e.g., [49]), such an arrangement is trivial (for instance, the interlocking behavior does not exist between elements of two neighboring stacks due to planar surface contact). To our knowledge, our work is the first approach to demonstrate a systematic design methodology for the volumetric decomposition of space with congruent prototiles.

1.3. Approach & Rationale

Our approach is rooted in Delone's (Delaunay's) work that developed a formal description for enumerating stereohedra [50]. However, Grünbaum and Shephard [24] later noted that while Delone's algorithm was the only effective algorithm known, it was practically infeasible. In fact, in the same work Grünbaum and Shephard also demonstrated that one could obtain congruent prototiles by using *symmetric Delone sets* (see section 2.1 for details), as Voronoi sites.

The *key idea* that forms the underlying basis for our proposed approach is the fact that the Voronoi decomposition [51] of symmetric Delone sets is indeed what results in plesiohedra [50]. A variety of shapes have already been identified as plesiohedral congruent polyhedra [52, 53, 24, 54] based on this observation. More interesting, even previous work on topological interlocking [11, 13] has invoked this principle without explicit reference to the Delone property. Having said that, an important conceptual tool these works offer is the utilization of higher-dimensional Voronoi sites such as lines, circles, and curve complexes that allow for interesting non-convex tiles instead of points that will always result in convex polyhedra. We use this idea to our advantage and demonstrate truly volumetric tiling (i.e. 3-honeycombs). Additionally, we show examples in which our 3-honeycomb, when *sliced* appropriately along specific planes, results in some of these existing 2.5D tessellations.

1.4. Contributions

The primary contribution of this work is a systematic computational methodology for the design of volumetric topologically interlocking space-filling tiles, including those with positive genus. The combination of the symmetric Delone property and higher-dimensional sites opens up a rich design space for cell-transitive 3-honeycombs. The important conceptual tool this work offers is utilization of higher-dimensional Voronoi sites such as lines, curves, and skeletons that allow for interesting handlebodies instead of points that will always result in convex polyhedra. We use this idea to our advantage and demonstrate truly volumetric topologically interlocking tessellations or 3-honeycombs.

To systematically demonstrate the richness of the design space of unchained handlebody plesiohedra, we focus our investigation on a small subset of the potential design space of all plesiohedra. This design space is generated by the isometries of a cube and a truncated octahedron as carefully selected subsets of the entire range of 3D space groups. In terms of the shapes of Voronoi sites, we only consider 3D line segments and un-linked circles. This choice is intentional since both shapes have only a few parameters that can be manipulated. This makes our design space extremely limited. For example, we can only change the center positions, orientations, and sizes of the circles. Despite these restrictions our results point to a large design space that is extremely rich yet intuitively controllable (Figure 12).

Using a subset of the shapes generated using cube isometries, we further investigate topological interlocking, which is our main design context. For this, we conduct a systematic analysis of a subset of the shapes produced using line sites (Section 5). Our analysis shows that we obtain the volumetric topological interlocking. To our knowledge, this is the first instance of space-filling and volumetric topologically interlocking tessellation (Figure 20). Our analysis further shows that the subsets of tiles on planes associated with the symmetry operation is also topologically interlocking (Figure 21).

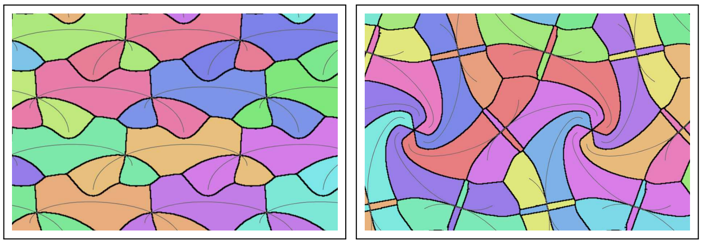

(a) *Intersected curves with pg symmetry.* (b) *Intersected curves with p6 symmetry.*

Figure 3: *Examples of intersected curves as Voronoi sites, which produce unacceptable cases.*

2. Conceptual Preliminaries & Background

Our conceptual framework for generalized plesiohedra is rooted in the concept of symmetric Delone sets, attributed to Boris Delone (Delaunay). The notion of Delone sets deals essentially with *well-spaced* sets of points. Let S denote a set of points in the n-dimensional Euclidean space, $\mathbb{R}^n$. The S is called a Delone set if it is uniformly discrete and relatively dense [55]. Formally, let $R > r > 0$ be two positive numbers. S is uniformly discrete if each ball of radius r contains at most one point in S. S is relatively dense if every ball of radius R contains at least one point of S [56]. If we used the points in $S \in \mathbb{R}^3$ as Voronoi sites, we would obtain 3-Honeycombs that contain *similar-sized* convex polyhedra as Voronoi cells. Due to this property, Delone sets and related Meyer sets have been used to define quasicrystal geometry [57, 58, 59, 60].

2.1. Symmetric Delone Sets

A Delone set S is symmetric if, for every two points $\mathbf{p}, \mathbf{q} \in S$, there exists a rigid motion of space that takes S to S and $\mathbf{p}$ to $\mathbf{q}$. The standard mathematical model of an ideal crystal also involves a specific type of Delone sets, called symmetric Delone sets [61, 62]. Symmetric Delone sets are invariant with respect to crystallgraphic groups [61]. Therefore, an ideal crystal structure can be described by a Delone set in n-dimensional Euclidean space along with a crystallographic group of Euclidean isometries acting at this point [50]. The principle underlying generalized Plesiohedra is that if a 3D arrangement of given a set of Voronoi sites is symmetric Delone, then the Voronoi tessellation results in a unique repeatable space-filling prototile. Note that the Voronoi sites need not be points, but can be higher-dimensional entities such as curves and surfaces in 3D space. With this in view, the main objectives of our conceptual framework are to (a) define an operator that produces an arrangement of Voronoi sites based on a given symmetry group and (b) enumerate and characterize the conditions under which the arrangement will be symmetric Delone.

To achieve this, we present a general approach (Section 3) for systematic exploration of handlebody tiling in $\mathbb{R}^3$ (i.e., 3-honeycombs) using Voronoi decomposition of high-dimensional sites. This approach may appear to work with any of the 230 spatial symmetries widely available in the literature [63, 64, 65]. However, it should be noted that many of the 230 space groups cannot be used in our approach since mirror operators do not produce the appropriate spatial arrangements to produce topologically interlocking solids with Voronoi decomposition [66].

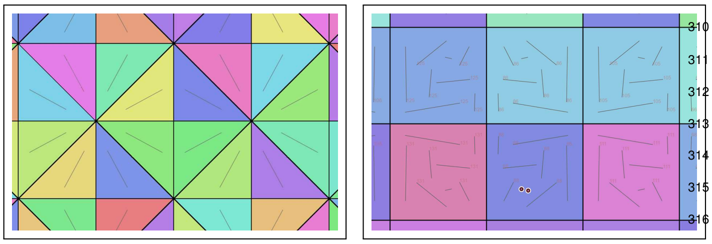

(a) *Example pattern with p4m symmetry.* (b) *Example pattern with pmm symmetry.*

Figure 4: *Wallpaper symmetry examples showing that symmetries that include multiple mirror operations cannot be used beyond classical plesiohedra construction. These images demonstrate that some symmetries always create the same polygon regardless of the complexity of the Voronoi sites. The p4m symmetry only creates Right Isosceles Triangles. The pmm symmetry does not create anything beyond square packing.*

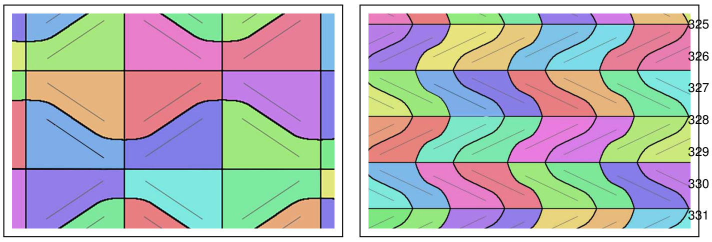

(a) *Example pattern with cm symmetry.* (b) *Example pattern with pmg symmetry.*

Figure 5: *Wallpaper symmetry examples showing that symmetries that include mirror operations cannot be used in topologically interlocking plesiohedra construction. These two examples show that some symmetries are not very useful since they cannot make all boundaries curved. Note that the cm and pmg symmetries always produce in straight infinite lines regardless of how we choose Voronoi sites.*

2.2. *Crystallographic Groups*

Crystallographic groups in 2D Euclidean space (i.e. 2D symmetry groups or wallpaper groups) have been very common and well known since antiquity. There is a strong discussion among mathematicians about whether there are all wallpaper symmetries in ancient architectural sites such as Alhembra [67, 68, 69]. Despite the widespread use of symmetric patterns in 2D in art and architecture, formalization of the symmetric patterns through rigid motions (or in other words, symmetry operations) did not start until the introduction of the Bravais lattice [70, 71] in 1850.

Sohncke listed the 65 space groups in 3D in 1880 [72]. Fedorov and Schoenflies further identified all 230 space groups in 3D by 1892 during a period of independent and collaborative work [73, 74, 75, 76]. The existence of 17 wallpaper symmetries was first identified by Fedorov in 1891 and was independently discovered by Polya in 1924 [63, 77]. Since then, a wide variety of notations have been developed to capture the nature of different symmetries, such as Schoenflies notation [74], Hermann-Mauguin notation [78], orbifold, and fibrifold notations [79, 80].

Today, extensive information is available on all crystallographic groups in a wide variety of sources [64, 65, 81]. Therefore, it appears to be straightforward to use crystallographic groups for creating arrangements that give symmetric Delone sets with higher-dimensional Voronoi sites. Unfortunately, all of these attempts primarily focus on enumeration and characterization rather than on the generation of symmetric structures. Those that do (for example [24]) are in 2D space.

2.3. *Symmetric Delone Sets with High Dimensional Sites*

The idea behind the generation of generalized plesiohedra is to take a discrete version of some higher dimensional geometric element (i.e. lines, curves, curve complexes, or even surfaces) and generate its spatial arrangement in such a way that the resulting point set is a symmetric Delone set. This can be achieved using the already known crystallographic groups to obtain such arrangements. In fact, this principle has already been utilized in a limited and implicit sense in several works to generate 2D and 2.5D space-filling tiles using wallpaper groups [11, 13, 14, 82, 83, 84, 85]. What we wish to do is to extend the idea to the 3D symmetry groups. Our extended framework, which subsumes these prior works, consists of the following four steps.

(1) We start with the initial Voronoi site. (2) We apply all transformations associated with a selected crystallographic group to obtain multiple copies of this site in the fundamental domain of the group. (3) We translate and copy the fundamental domain containing the site copies in 3-space to obtain a uniformly discrete and relatively dense set (Figure 1a). (4) We select a copy of the initial Voronoi site that is surrounded by other copies.The point set obtained from these four steps, when used as labeled sites for Voronoi tessellation (Section 3), will result in an assembly of plesiohedral shapes (Figure 1b).

While the steps above seem straightforward, making them work for generating topologically interlocking tessellations is not trivial. Of course, the use of higher dimensional sites (lines and circles in our specific investigations) opens up the possibility for interlocking. However, not all spatial symmetry groups are amenable to generating topological interlocking properties. Furthermore, recall that our goal is to create cell-transitive 3-Honeycombs, meaning that all prototiles should be congruent and topologically interlocking simultaneously. To achieve this, two requirements must be met. First, the exact (necessary and sufficient) number of site copies, that are unique, (step 2) must be generated to ensure symmetric Delone condition necessary for congruency. Second, we must avoid crystallographics groups involving mirror operations to ensure topological interlocking. Below, we discuss the rationale for these two requirements in detail.

2.3.1. *Guaranteeing Unique Copies of Sites*

To satisfy the uniformly discrete and relatively dense properties of the Delone set, it is critical to produce **all (sufficient) and only (necessary)** copies of the initial Voronoi site. Let us call these unique copies. For example, consider that a symmetry operation includes only the rotation of 120^0. We need to apply this operation exactly three times to obtain three unique copies of the initial Voronoi site. If we apply this operation less than three times, we will not produce all copies and the resulting set will not be relatively dense.

If we apply the operation more than three times, we produce more copies than necessary and the resulting set will not be uniformly discrete, that is, there will be multiple copies at the same locations. This means that even though these sets can appear to be closed under the crystallographic group the resulting point set is not Delone. Now, in the discrete case, this problem manifests itself in the form of intersecting regions after Voronoi tessellation, which is unacceptable (Figure 3).

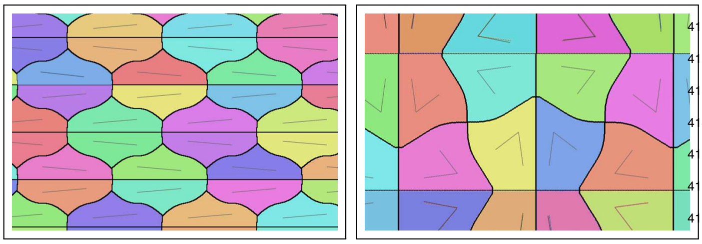

(a) *Example pattern with pgg symmetry.* (b) *Example pattern with p4g symmetry.*

Figure 6: *Wallpaper symmetry examples showing that symmetries that include glide reflection operations cannot be used in topologically interlocking plesiohedra construction. Note that glide reflections also always produce in straight infinite lines regardless of how we choose Voronoi sites.*

2.3.2. *Avoiding Mirror Operation*

In our applications, we essentially want our shapes to possess topologically interlocking property [86, 15, 3]. Topologically interlocking blocks do not have contact boundaries that can allow groups of blocks to slide under peripheral constraints. The problem is that the symmetry groups that include mirror operations cannot provide topological interlocking [66]. Furthermore, symmetry groups involving multiple mirror operations are even worse since they result classical space-filling solids (cube, hexagonal prism, rhombic dodecahedron, or truncated octahedron) regardless of the shapes of the initial Voronoi sites. The 3-Honeycombs of these solids is not topologically interlocking. This problem is even visible with wallpaper groups, as shown in Figure 4. Even if there is only one mirror operation, the resulting plesiohedra are not topologically interlocking; plesiohedra boundaries can form a single infinite plane that can allow sliding as shown in Figure 5. Although single glide reflection is not a problem, multiple glide reflections can also produce a single infinite plane that can allow sliding, as shown in Figure 6. In wallpaper groups, only six of all 17 groups, namely, p1,pg, p2,p3,p4, and p6, are useful. The other 11 wallpaper groups cannot be used to generate 2D topologically interlocked plesiogons (2D plesiohedra). In the same way, not all 3D crystallographic groups will lead to topologically interlocked space-filling tiles. To address this, our goal is define a systematic approach to intuitively identity subsets of these groups that will guarantee topological interlocking.

2.4. *Choice of Cystallographic Subgroups using Cube Isometries*

In order to develop an intuitive way of generating symmetric Delone arrangements specifically for topologically interlocking assemblies of space-filling tiles, for choose to use the isometries of the cube. As a means of demonstrating the generality of our conceptual framework, we also show an example based on the isometries of a truncated octahedron (Figure 15). Our choice of cube isometries is based on its simplicity and richness of the corresponding symmetry groups. Note that we focus only on non-mirror symmetry groups based on isometries of a cube. The main reason for this restriction is that operations such as mirror are not useful for obtaining topologically interlocking assemblies (Section 2.3.2).

The cube has a total of 24 rotational symmetries, which, when combined with reflection, result in a total of 48 symmetries. There are different ways of enumerating the elements of the symmetry group of the cube, the most common being the direct product ($O_h = S_4 \times Z_2$) of the *symmetric* group S_4 of the sets of 4 elements and the cyclic group Z_2. However, the representation most amenable to our work stems from the crystallographic parlance that constructs a relationship between the symmetry group of a cube and the cubic lattices. Given a unit cube C in three-dimensional Euclidean space, we begin by enumerating the set of axes that generate the rotational symmetries of C as follows:

- Four vertex-centered/body diagonals ($\hat{\mathbf{b}}_\mathbf{0}, \ldots, \hat{\mathbf{b}}_\mathbf{3}$) that enumerate rotational symmetries through rotations by 120^o (Figure 7(a)).
- Six edge-centered diagonals ($\hat{\mathbf{e}}_\mathbf{0}, \ldots, \hat{\mathbf{e}}_\mathbf{5}$) that enumerate rotational symmetries through rotations by 180^o about the diagonals (Figure 7(b)).
- Three face-centered diagonals ($\hat{\mathbf{f}}_\mathbf{0}, \ldots, \hat{\mathbf{f}}_\mathbf{2}$) that enumerate rotational symmetries through rotations by 90^o and 180^o (Figure 7(c)).

The inversion operation ($M : (x, y, y) \mapsto (-x, -y, -z)$) in conjunction with the above results in a total of 48 cube isometries. In our work, we use this information to develop "*arrangement operators* ($\mathcal{A}$)" that combine the rotational symmetries induced by the axes enumerated above with a copy operation to produce a pattern of a seed geometry.

3. Tile Generation Methodology

In order to generate generalized plesiohedra for a given arrangement of sites, we utilize the approach offered by recent works [14, 13]. The broad idea is to sample a set of points on a given high-dimensional Voronoi site (in their case, line segments or surfaces), compute the tessellation with the sampled points as sites, and finally construct a union of the Voronoi cells corresponding to the points that belong to the same high-dimensional site. We chose this approach in contrast to alternatives such as voxel-based (implicit surface) methods owing to its simplicity of implementation and computational efficiency. Our results can be obtained from any standard modeling package that supports robust 3D Voronoi tessellation for points. Given that this approach directly uses Voronoi tessellation, it guarantees a watertight assembly of tiles wherein each resulting tile is identical (up to its piecewise linear approximation resulting from the union). The tile generation process is straightforward and consists of a few number of steps.

1. *Choose an initial Voronoi site shape:* The initial Voronoi site can be any 3D shape. Figure A.23a shows a single line as the initial Voronoi site.
   Remark on 3D Shapes of Voronoi sites: In the examples of this paper, we particularly focus on curves and curve-complexes as Voronoi sites to evaluate the design space effectively. Moreover, we do not allow knotted curves [87] to avoid additional complexity of evaluation.
   Remark on sizes of Voronoi sites: In this paper, Voronoi sites are completely inside of the cube C of unit length centered at $[0\ 0\ 0]^T \in \mathbb{R}^3$ to avoid potential complexity obtaining single tile (See step 3).

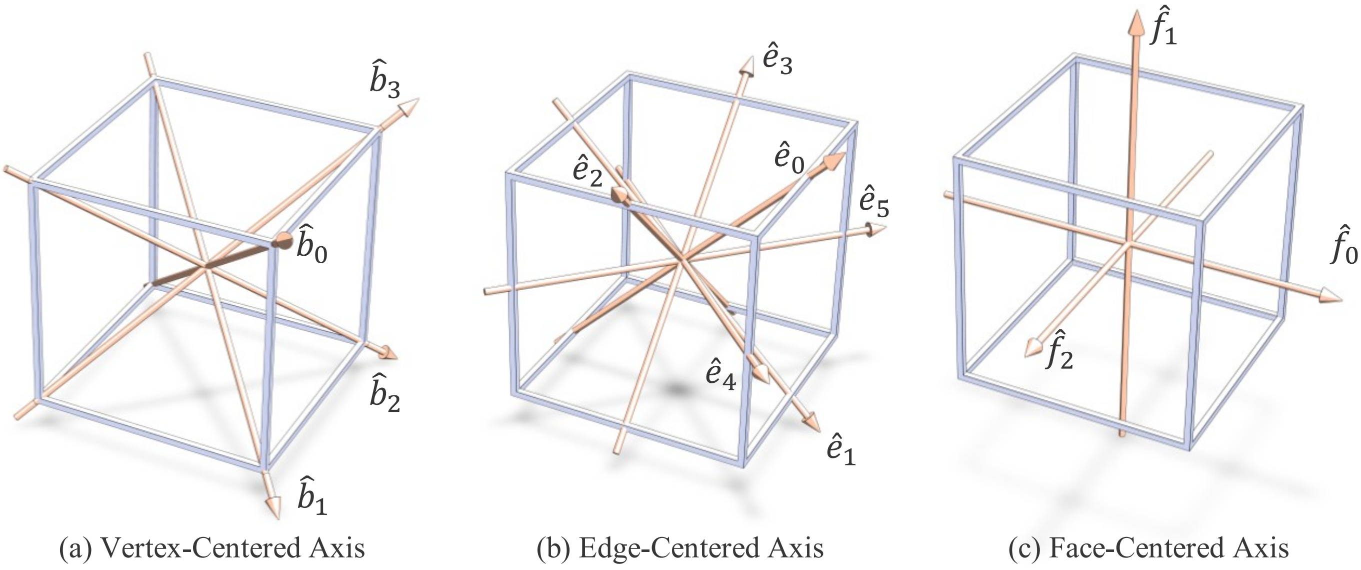

Figure 7: Rotations about the vertex-, edge-, and face-centric axes preserve the orientation of the cube.

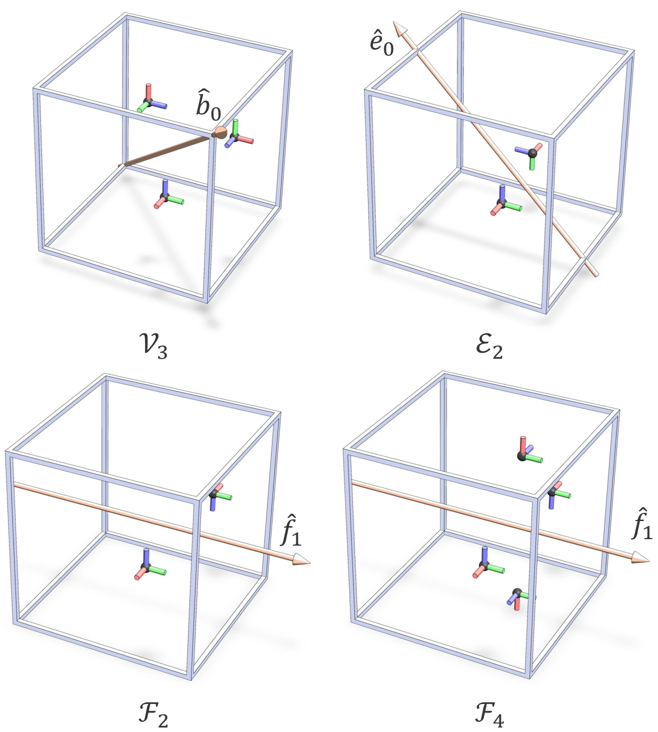

Figure 8: Examples of arrangement operators with their symmetry axis and the patterned coordinate frames.

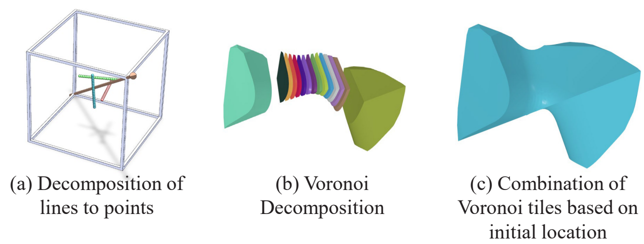

Figure 9: A demonstration of the process of deconstructing lines into points and using the points as Voronoi sites to create polyhedral volumes with planar faces and straight edges. The union of these polyhedral volumes provides the generalized Plesiohedra tile.

2. *Apply arrangement operators:* Applying a given set of arrangement operators to initial the initial site creates multiple copies of the initial site as shown in Figure A.23b.
   Remark on Symmetry: Since we view the original cube as a 3-Toroid, this process theoretically give us a symmetric set in 3D Euclidean domain.
   Remark on Delone Property: To satisfy Delone property, the final sites must not intersect with each other, which can be computed using a distance comparison on the point sites up to a threshold.
   Remark on for closed curves: To guarantee the assembly of final tiles, the copies of the 'closed curves must not form links [87].

3. *Translate to create* $3 \times 3 \times 3$ *copies:* A practical representation of the 3-Toroid can be obtained by $3 \times 3 \times 3$ translated copies of the original cube as shown in Figure A.23c. This subset is obtained by translating the multiple set of Voronoi sites that are obtained by arrangement operators.
   Remark on Translation: These 27 copies include all potential neighbors of the original Voronoi site for any symmetry operation if the original shape is guaranteed to be in the original cube. However, in general depending of the shape of the initial Voronoi site, more copies may be needed.

4. *Compute Voronoi Decomposition:* Voronoi diagram is computed using all copies of the original Voronoi site. Voronoi cell that corresponds the original Voronoi site provides desired tile (See Figures A.23d and A.23e). To compute the Voronoi decomposition for higher dimensional sites, we

employ a used method that provides a piecewise linear approximation of the desired Voronoi cell [13, 14]. This allows us to not compute the Voronoi diagram in the continuous case but rather on a discrete set of points. The process consists of three steps:

(a) *Sample Voronoi Sites:* Sample all Voronoi sites using points as shown in Figure 9.

(b) *Classify Points into two categories:* Classify all the points sampled from the original Voronoi site using the same label, say 0. The rest is labeled with a different label, say 1.

(c) *Decompose the space by inheriting labels:* Decompose the space using these points as Voronoi sites. This process creates a set of Voronoi cells as polyhedral shapes with planar faces and straight edges. Each Voronoi cell inherits the label of its corresponding Voronoi site.

(d) *Take Union:* Take the union of all Voronoi polyhedra with the same label. This gives us two shapes: the generalized Plesiohedral tile and its mold (in other words its complement). The tile comes from the union of all polyhedra labeled 0. The mold comes from union of all polyhedra labeled 1.

4. Site Design: Generation of tiles using a variety of sites

There are a wide variety of sites that can be used to generate different plesiohedra. The choice of site geometry can significantly influence the shape of a plesiohedral prototile. In order to understand the relationship between site geometry and the resulting plesiohedra, we conducted experiments with three different site geometries, namely, straight line segments, circles, and curve-complexes.

4.1. Lines

The simplest extension to typical plesiohedron is the use of lines as sites (Figure 10). Using line segments allows a relatively simple evaluation of the impact on the shapes from the Voronoi sites. An advantage of using a line segment is that it can be defined only with a small number of parameters. We have evaluated the impact of three types of geometric parameters, namely the length, the angle, and the initial placement of the line. This helps to evaluate the effect of these parameters. For instance, as the length of the line site decreases, the high dimensional Voronoi Sites turn into single points, and the resulting Voronoi polyhedra approach a classical plesiohedron.

The length and angle parameters of the starting line give rise to a rich design space, which could potentially result in interesting mechanical properties. For example, for a certain type of symmetry operator, changing the angle parameters may increase or decrease the amount of energy absorption the tiles posses. Similarly, the length parameter may increase or decrease the topological interlocking capabilities for an assembly. To that effect, we performed a use case test on topological interlocking analysis using line sites (see Section 5).

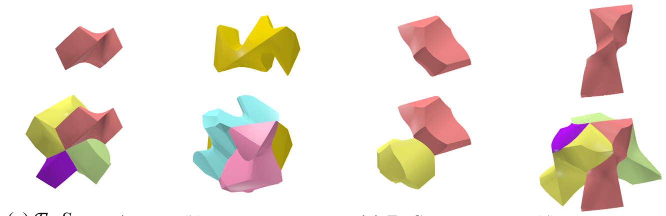

(a) $\mathcal{F}_4$ Symmetry Operator (b) V_3 Symmetry Operator (c) E_2 Symmetry Operator (d) $\mathcal{F}_4$ Symmetry Operator

Figure 10: A single line was used as an initial site with various lengths, angles, and placement as well as different operators.

Figure 11: The effect of changing the radius of a circle Voronoi site in combination with the $\mathcal{F}_4$ operator is shown. This change causes a change of topology by opening and closing a hole in the resulting tiles.

4.2. Circles/Curves

One can imagine the generation of our tiles as a result of concurrent "*growth*" of each site until the growing volume meets neighboring volumes that are also growing (this is indeed a known physical characterization of Voronoi partitioning in general). To create higher genus sites, it is natural to consider sites containing cycles, the simplest example being a circle. Using circles as Voronoi sites is also useful for evaluating our approach since there are, again, only a few geometric parameters to define the shape of the circles. We use the radius, 3D orientation, and center of the circle as geometric parameters to specify the site geometry. The use of circles also allows for the creation of positive genus tiles. We demonstrate that we can obtain positive genus tiles regardless of symmetry operators (Figure 12). It is important to note that the circle parameters must still be intelligently designed. Any arbitrary circle shape may not create a positive genus tile. This is obvious, especially for small circles that are distant from each other. As the radius of circles decreases, the sites again approach single point sites, and the resulting Voronoi polyhedra approach the classical convex planar plesiohedron. For instance, when the $\mathcal{F}_4$ operator is used, the plesiohedron produced by the decreasing radius of the circles approaches a rectangular prism (Figure 11). On the other hand, as the radius of the circle increases, a hole is created in the center of the tile (Figure 11).

4.3. Curve Complexes

The generation of Plesiohedral tiles with lines and circles can be directly extended to more complex site designs (and hence a diverse variety of tiles) through simple skeletal combinations. One example of this is a planar site design with four radial lines on a single circle arranged symmetrically (Figure 13). Given appropriate choices of the lengths of the lines and the circle's radius, this site design results in a genus-1 tile with some unique protruding features resulting from the lines. Another example of connected line sites is using the medial axis of common shapes. The medial axis of an isosceles triangle, square, and tetrahedron

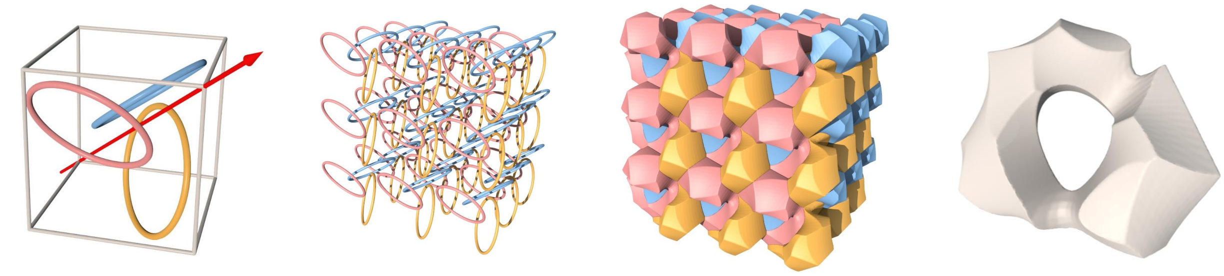

(a) Circle Site chosen and $\mathcal{V}_3$ operator used

(b) Patterned using cube translation

(c) Assembly of Unit Tile

(d) Unit tile

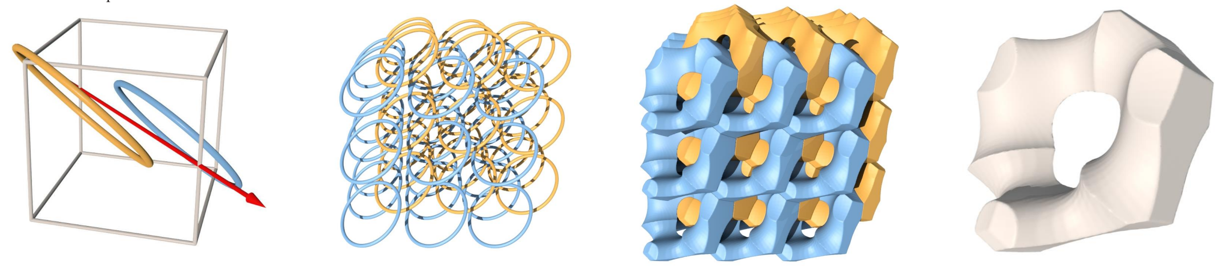

(e) Circle Site chosen and $\mathcal{E}_2$ operator used

(f) Patterned using cube translation

(g) Assembly of Unit Tile

(h) Unit tile

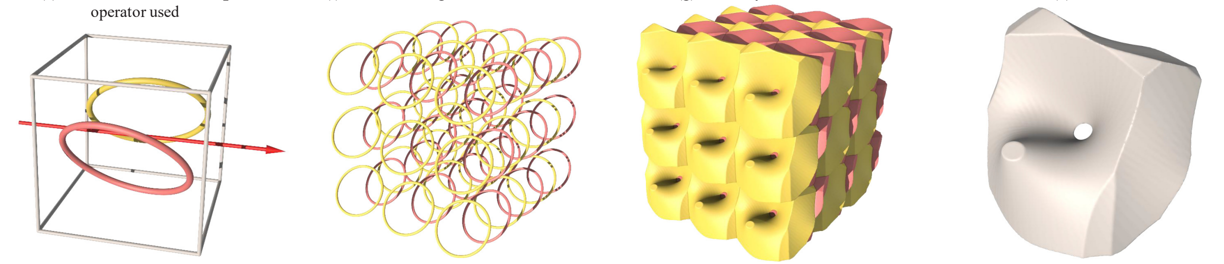

(i) Circle Site chosen and $\mathcal{F}_2$ operator used

(j) Patterned using cube translation

(k) Assembly of Unit Tile

(l) Unit tile

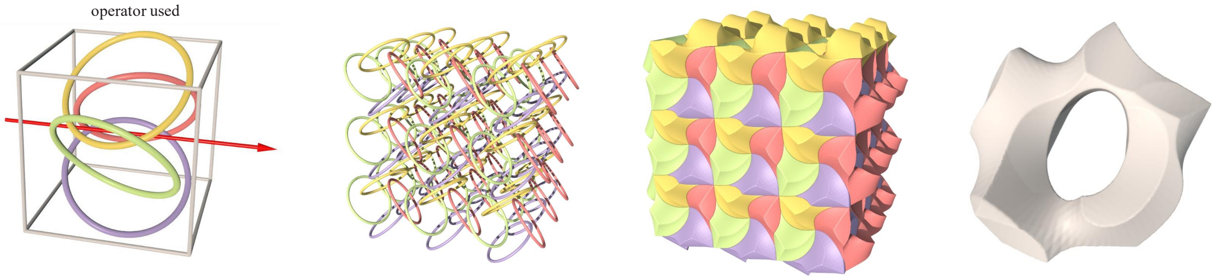

(m) Circle Site chosen and $\mathcal{F}_4$ operator used

(n) Patterned using cube translation

(o) Assembly of Unit Tile

(p) Unit tile

Figure 12: We show examples of genus-1 space-filling tiles using our method of applying a given operator(a,e,i,m) and patterning to obtain a grid of sites(b,f,j,n). Then the Voronoi tessellation can be created, and an assembly of tiles is shown (c,g,k,o). Additionally, a single unit tile from the assembly is pictured to show the genus of the tile (d,h,l,p)

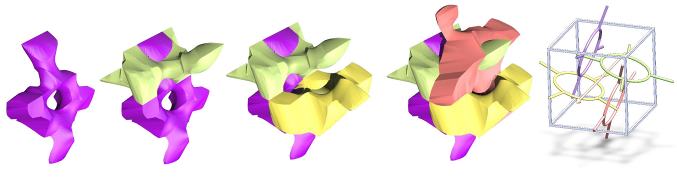

Figure 13: A circle with 4 lines was used as the initial site with the $\mathcal{F}_4$ operator. The resulting tile is shown and is genus-1.

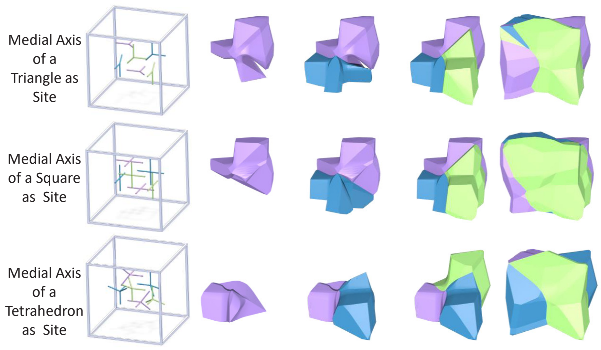

Figure 14: The medial axis of several common shapes are used as the sites using $\mathcal{E}_2 \circ \mathcal{V}_3$ to create the tiles. The first set of sites are the medial axis of a triangle, square, and tetrahedron.

can be utilized with the $\mathcal{E}_2 \circ \mathcal{V}_3$ operators to create complex tiles (Figure 14). This site design allows for the creation of tiles that cannot be obtained with single line segments or circles.

4.4. Other Space Filling Polyhedra

Although we focused on the cube isometries to create generalized plesiohedra, other space-filling polyhedra (triangular prism, hexagonal prism, gyrobifastigium, and truncated octahedron) can be used to define arrangements of sites resulting in generalized Plesiohedra. To do so, all that needs to be done is to define arrangement operators based on the isometrics of a given space-filling polyhedron. For instance, the isometries of a truncated octahedron may include rotational symmetries based on opposite faces and vertices. Creating arrangements based on these isometries result in 3-honeycombs (Figure 15) simply by following the same procedure (i.e., enumeration of arrangements closed under a given rotational symmetry). A complete enumeration of the closure properties for other space-filling convex polyhedra can be easily developed, similar to the cube isometries shown in this work. It may also possible that using specific space-filling polyhedra could offer unique access to a specific design space of the resulting plesiohedron.

5. Case Study: Topological Interlocking

Our study with site design reveals a few special combinations of site geometry and arrangement operator leading to some practical applications. We specifically explored a case study based on topologically interlocked tiles, that are well-known for desirable mechanical properies such as high energy absorption and fracture toughness [3]. Specifically, we observed that the orientation of line sites results in surface contacts with saddle points which has been shown to induce topological interlocking. However, our case is distinct from previous works [11, 13] in that generalized Plesiohedra are volumetric. As a result, they have the potential ability to be topologically interlocking along multiple directions as well as on multiple planes (slices of the 3D volume). In fact, our approach can be used to generate both Delaunay Lofts [11] as well as generalized Abeille tiles [13] as special cases as well. To explore this possibility, we present a case study to investigate design parameters of line sites for generating topologically interlocking tiles.

We constrain our investigation to a parametric variation of the orientation of a single line segment and evaluate parameter ranges where we observe interlocking behavior. To define the orientation of the line segment, we use a plane that contains the axis of symmetry and the site parallel to the axis of symmetry. The ϕ axis can then be defined to be on that plane as well as being perpendicular to the axis of symmetry(Figure 16). Furthermore, the θ angle is defined to be perpendicular to the site and the ϕ axis(Figure 16). This axis definition means that any rotation about either axis gives non-parallel sites. We observed that having non-parallel sites helps to obtain strong interlocking. This exploration allows for a wide number of plesiohedron that can be created with various operators (Figure 17). For our case study we constrain our analysis to the orientation parameters (θ and ϕ) of a single line site.

Consider an arrangement operator $\mathcal{A}$ with a symmetry axis $\hat{\mathbf{a}}$ consider the line parameters $0^o < \theta < 90^o$ and $0^o < \phi < 90^o$. Under these conditions, our ***first working hypothesis*** is that a sub-assembly of tiles arranged on a plane orthogonal to $\hat{\mathbf{a}}$ will be topologically interlocking (Figure 18). Our ***second working hypothesis*** is that for a composition of multiple operators, if the same conditions are satisfied for both operators, the sub-assembly of tiles arranged on a plane orthogonal to either of the multiple axes will be topologically interlocking. Even though it is possible to confirm these hypotheses through visual inspection, 3D space symmetries are complex and often may lead to results that may be counter-intuitive. Therefore, we conduct an algorithmic analysis to confirm our hypotheses as described below.

5.1. Interlocking Evaluation

Most previous work on topological interlocking [3] has studied the interlocking properties experimentally. Work by Jiang et al. [44] was among the first to integrate physics-based evaluation to generate optimal topological interlocking on surfaces. Our aim in this analysis is mainly to test our hypotheses which are predicated on the question: *given some "central" tile in a planar sub-assembly in a volume, is the central tile topologically interlocked?* Here, a "*central*" tile is simply a tile that is partially surrounded by other "*neighboring*" tiles that are fixed in space.

Note that the interlocking of a given central tile is fundamentally dictated by the geometry of contact between neighboring tiles. Specifically, this is a question of the *form closure* of a central tile, given a set of surfaces in contact with the neighboring tiles. For the concept of the form-closure in robotics literature, please see [88]. Based on this observation, our original question can be re-formulated as: *what is the degree-of-freedom (DoF) of a given central tile if its contact surfaces with the peripheral tiles are restricted to move?* A tile is interlocked if $DoF = 0$, i.e., it is immovable under the surface contacts imposed by its

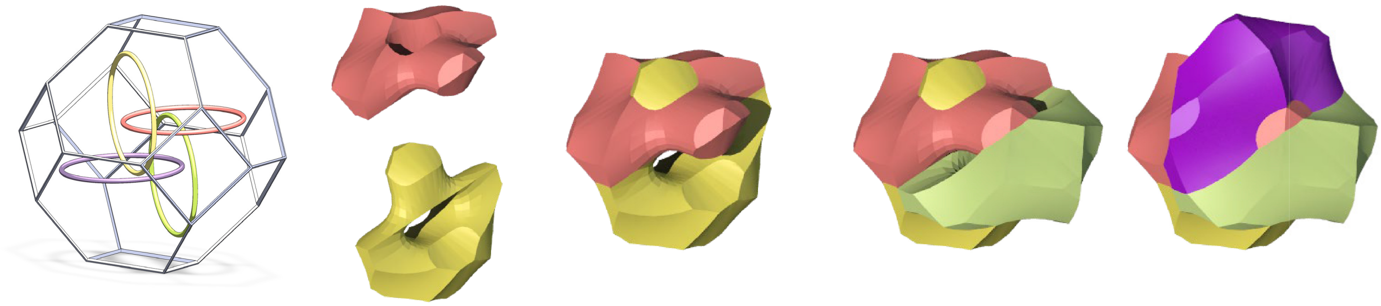

Figure 15: An example of a plesiohedron generated using a truncated octahedron to pattern the initial sites as well as the sites after an $\mathcal{F}_4$ operation.

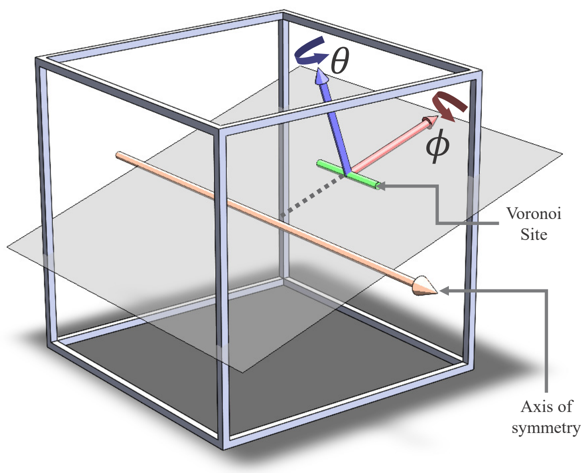

Figure 16: The vectors used to define angle rotation is shown for the $\mathcal{F}_4$ operator. The ϕ axis is in the direction of the center of the site to the symmetry axis and the θ axis is perpendicular to the ϕ while also being on the plane perpendicular to the symmetry axis. A transparent plane is shown to help visualize the axis direction and position.

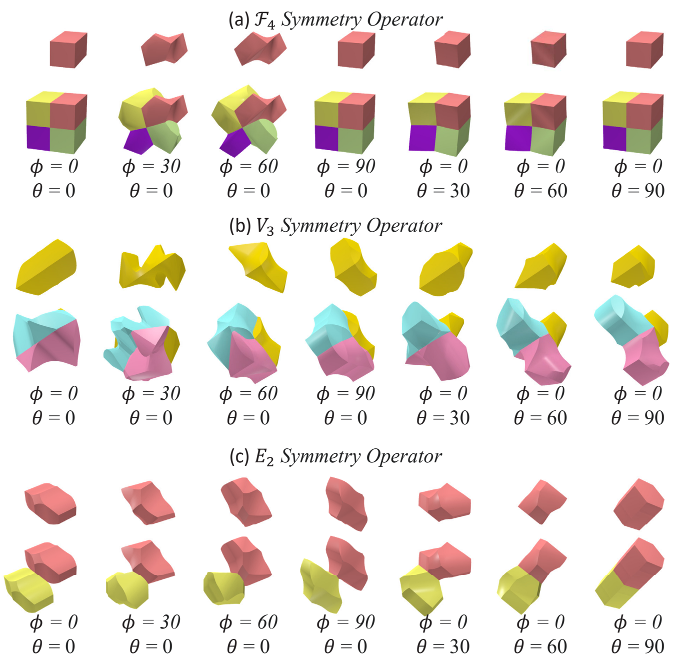

Figure 17: The differences of tiles where the angles of rotation are varied. The initial line was made parallel to the axis of rotation (Figure 16).

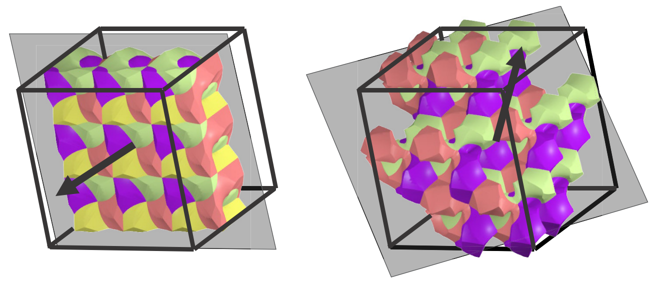

(b) F_4 Symmetry axis (d) V_3 Symmetry axis

Figure 18: For the DoF analysis only tiles that intersect with a plane perpendicular to the symmetry axis are taken. These tiles are shown for the two operator case to help visualize the orientation.

neighboring tiles. *Note that in this study, we only consider translational degrees of freedom, i.e., we assume that the tile cannot be rotated.*

In order to computationally determine the DoF of the central tiles, we take inspiration from the notion of form-closure, i.e., immobility of an object under kinematic (purely geometric) constraints. While there is extensive kinematics literature on form closure for point contacts [89], the treatment of higher kinematic pairs (curve and surface contacts) is relatively less understood. To answer our question, we formulated our problem as a linear programming problem wherein we model the contact surfaces as the constraints ($A\mathbf{x} \leq \mathbf{b}$) and each of the unrestricted surfaces ($f^T\mathbf{x}$, where f is the coefficient vector) as the objective functions to be minimized (see Appendix Appendix B for details).

5.2. *Experimental Methodology*

Continuing our design study rationale, we tested our hypotheses using lines as Voronoi sites. Our aim was to study the relationship between the line orientation and the DoF against different arrangement operators. Therefore, we conducted a parametric investigation for each operator individually for our first hypothesis (Figure 19). We also study one example for a composition of two operators to test our second hypothesis (Figure 21). The following are the steps for each individual arrangement operator:

1. Define a line of a fixed length at a fixed location in the cube.

2. Apply the arrangement and generate plesiohedral tiling.

3. Determine all tiles that intersect the plane normal to the symmetry axis of the operator. These tiles define a sub-

tiling. For example, for the operator $\mathcal{V}_3$, the plane is normal to the axis $\mathbf{b}_j$ and passes through the center of one of the cubes.

4. Identify a tile in the sub-tiling that has a complete neighborhood of tiles on the plane. This is the central tile.
5. Construct the constraints based on the faces of the central tile that are in contact with the neighboring tiles.
6. For each unrestricted face (i.e. a face on the central tile not in contact with a neighboring tile), construct the objective function and determine the optimum (if one exists in the feasibility region defined by the constraints).
7. Compute the DoF of the central tile based on the optima obtained from the linear program for the unrestricted face.

In the case of a composition of operators, we use this methodology for the normal planes associated with each of the symmetry axes independently.

5.3. Key Findings

In general, both our working hypotheses were confirmed in our analysis for $\mathcal{F}_4$ symmetry operator as expected. For example, the DoF of a central tile is 0 for when $0^o < \phi < 90^o$ the result is an interlocked tile (Figure 19). This is because all of the contacts between adjacent tiles are non-planer when $0^o < \phi < 90^o$. However, when $\phi = 90^o$ or $\phi < 90^o$ the sites are all parallel or lie on a singular plane which allows for complete removal of the central tile along the vector that defines the symmetry axis.

Interestingly, in case of the $\mathcal{V}_3$ operator, the central tile is immovable even when $\phi = 0^o$ and $\theta = 0^o$. The only time that the central tiles is movable (DoF > 0) is when all of the sites lie on the same plane. This condition occurs when either $\phi = 90^o$ or $\theta = 90^o$ (Figure 20) and all the contact surfaces with the neighboring tiles have no component in the direction of the axis of rotation which allows for removal along that direction.

Another important observation we make is that in both the examples above, varying θ does not change the number of of adjacent tiles that a given tile is in contact with. In the case of $\mathcal{F}_4$ a central tile is only ever in contact with four tiles for any $\phi = 0^o$. Similarly with $\mathcal{V}_3$ for any $\phi = 0^o$ a tile is only in contact with with six other tiles. Even though this seems obvious, we should note that this property may be affected by the assumption that the initial Voronoi site (the line) is appropriately sized (such that it is contained within the cube).

Even though we had expected to see interlocking sub-tiling for a single operator, we were expecting to face issues with compositions of multiple operators. However, our second working hypothesis was also confirmed in our analysis. For example, the composition $\mathcal{F}_2 \circ \mathcal{E}_2$ results in a unit tile which has many more curved faces than that of a tile that had just one of the operators. This property helped to ensure that tiles were topologically interlocked. These tiles also have two 2.5D assemblies about each of the planes perpendicular to each symmetry axis (Figure 21). In the case of compositions of multiple operators the number of neighboring tiles for a given central tile is obviously higher than that with a single operator. This results in more non-planar surface and edge contacts between tiles, thereby increasing the avenues for interlocking.

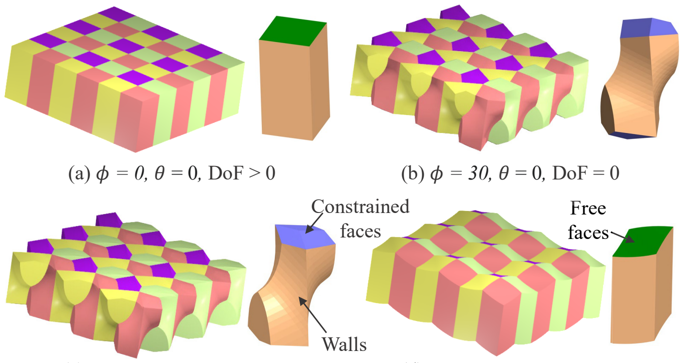

(a) ϕ = 0, θ = 0, DoF > 0 (b) ϕ = 30, θ = 0, DoF = 0
(c) ϕ = 60, θ = 0, DoF = 0 (d) ϕ = 0, θ = 60, DoF > 0

Figure 19: DoF is shown for varying angles with respect to the $\mathcal{V}_3$ arrangement operator (Figure 17 a)).

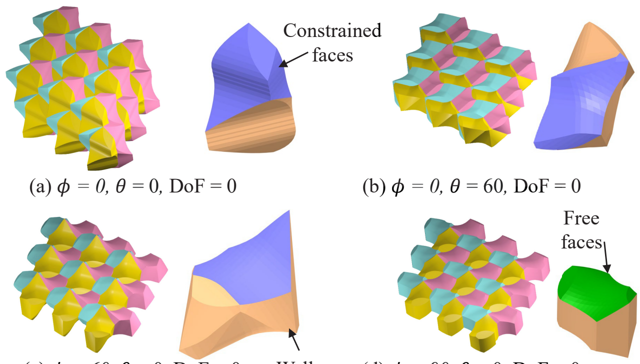

(a) ϕ = 0, θ = 0, DoF = 0 (b) ϕ = 0, θ = 60, DoF = 0
(c) ϕ = 60, θ = 0, DoF = 0 (d) ϕ = 90, θ = 0, DoF > 0

Figure 20: DoF is shown for varying angles with respect to the $\mathcal{V}_3$ arrangement operator.

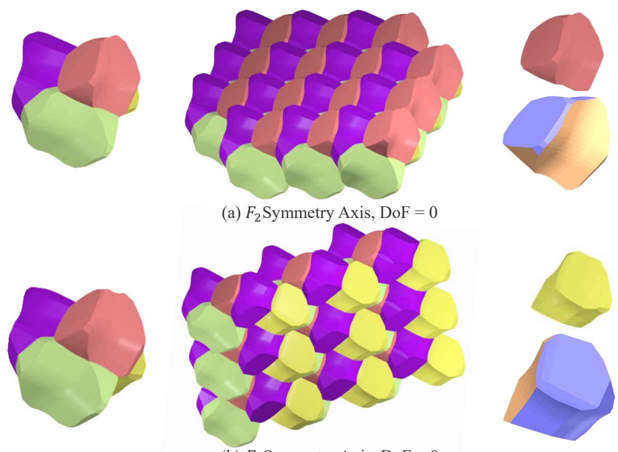
(a) F_2Symmetry Axis, DoF = 0
(b) E_2Symmetry Axis, DoF = 0

Figure 21: The Degree of Freedom (DOF) analysis was conducted on the tile created using a line segment and two operators $\mathcal{F}_2 \circ \mathcal{E}_2$. An assembly was taken along each of the two planes perpendicular to each of the two symmetry axis. The central tile could then be analyzed to determine it's DoF. The assembly of 4 tiles is also shown.

6. Limitations & Future Directions

We present a systematic approach for generating generalized Plesiohedra. To our knowledge, this is the first approach to operationalize the spatial symmetry principles well-known in the domains of geometry, algebra, crystallography, and other domains in order to explore the rich and untapped design space of cell-transitive 3-honeycombs. However, there are some limitations of this approach as presented in this paper. First, because of the involvement of Voronoi tessellations, the relationship between the input sites and the resulting tiles may not be obvious to the user. However, the ability to quickly create and edit sites of arbitrary complexity may help mitigate this limitation. Secondly, the current paper has focused primarily on cube isometries which are a subset of spatial symmetry groups as enumerated by Federov and Schoenflies [63]. Although we have demonstrated an example with a truncated octahedron, more work is needed to extend the methodology using other Bravais lattices [70, 71]. It will also be important to generalize the method to Wigner-Seitz cells [4], especially the five topologically distinct parallelohedra [90]. Finally, our current investigation focused on line and circle sites, while only superficially exposing other alternatives (e.g. skeletal geometry). We believe that more careful exploration is needed with more complex sites to establish an intuitive relationship between site design and the resulting tiles.

Having said all this, we see several avenues for future work. First, the ability to systematically design complex cell-transitive honeycomb structures can be powerful in designing materials with a wide range of mechanical properties. There is a need to explore domain-specific mechanical metamaterial applications for a variety of subclasses of tiles (symmetry-site combination). In principle, since the set of all possible arrangements is finite, it is easy to see that one can pre-compute and tabutale the operators and generate generalized plesiohedra. However, note that relaxing the closure property on the arrangement operator can be used to generate volumetric tessellations with a finite set of unique prototiles. A particular advantage of Voronoi-based design is that topology optimization for multi-material systems can be simplified owing to the simple skeletal representation of the input geometry in the form of Voronoi sites. Instead of directly dealing with complex 2-manifold shapes, we can simply change the topology of the Voronoi sites.

From practical point of view, the main advantage of our methodology is to allow the creation of a wide range of unchained handlebody plesiohedrons through a few parameters. Even using a limited number of crystallographic groups, we have shown that it is possible to obtain a wide range of shapes with various combinations of symmetries and site design. Our results suggest that the parameteric space of the family of space-filling handlebody shapes is quite large. We want to point out that we can also increase parameteric space of higher dimensional Voronoi sites by replacing lines and circles with curve complexes, i.e. 3D graphs with curved edges. Therefore, designing and building a wider variety of tiles of positive genus can be quite easy.

7. Conclusion & Future Work

Although we demonstrated the approach with line segments and circles as Voronoi sites, it is straightforward to extend the design approach to any 3D shape such as curves, curve complexes, surface patches, surface-patch complexes, and a mixture of any of these entities. A similar method of sampling the continuous case into a discrete set of points can be used in this to simplify the generation process. We want to point out that most of our observations about the effect of positions, orientations, and sizes of line segments and circles are generally applicable to other Voronoi sites. For example, as the sizes increase, the expectation of increasing concave surface contacts would still hold. Similarly, orientations will also strongly dictate the strength of interlocking between neighboring tiles. By changing sizes and orientations, we can open and close holes, thereby changing the genus. On the other hand, studying a specific type of 3D shape can still be useful and provide unexpected properties.

We explored one potential use case for generalized plesiohedra by creating topologically interlocked assemblies. It was also shown that there exist parameters of the sites that can influence whether an assembly is topologically interlocked or not. We believe that the generation methodology presented in this work will help in the further development of complex topologically interlocked assemblies. Furthermore, it is possible to develop a methodology to create graded topologically interlocking assemblies in one or multiple directions by changing the parameters of the sites along multiple axes.

This work also provides a systematic way to generate positive genus congruent tiles. Although there is work on generating prototiles of positive genus [47, 49], they demonstrate singular instances to generate specific types of tiles rather than a design space of such tiles. For example, [49] is primarily an extension of a previous work on topologically interlocking tiling rooted in Joseph Abeille's structures [13]. In contrast, our methodology offers unprecedented access to the design space of tiles of higher genus through the use of isometries of space-filling polyhedra. Overall, this work opens up interesting avenues for computer-aided design of complex geometric forms with potential applications in engineering, architecture, and art.

Acknowledgement

This material is based upon work supported by the National Science Foundation under Grant No. #2048182. Any opinions, findings, conclusions, or recommendations expressed in this material are those of the author(s) and do not necessarily reflect the views of the National Science Foundation.

References

[1] Y. Matsumoto, An introduction to Morse theory, Vol. 208, American Mathematical Soc., 2002.

[2] A. L. Loeb, Space-filling polyhedra, in: Space Structures, Springer, 1991, pp. 127–132.

[3] Y. Estrin, V. R. Krishnamurthy, E. Akleman, Design of architectured materials based on topological and geometrical interlocking, Journal of Materials Research and Technology 15 (2021) 1165–1178.

[4] E. Wigner, F. Seitz, On the constitution of metallic sodium, Physical Review 43 (10) (1933) 804.

[5] M. Ashby, The properties of foams and lattices, Philosophical Transactions of the Royal Society A: Mathematical, Physical and Engineering Sciences 364 (1838) (2006) 15–30. doi:10.1098/rsta.2005.1678.
[6] J. Martínez, J. Dumas, S. Lefebvre, Procedural voronoi foams for additive manufacturing, ACM Transactions on Graphics (TOG) 35 (4) (2016) 1–12.
[7] J. Martínez, H. Song, J. Dumas, S. Lefebvre, Orthotropic k-nearest foams for additive manufacturing, ACM Transactions on Graphics (TOG) 36 (4) (2017) 1–12.
[8] J. Martínez, S. Hornus, H. Song, S. Lefebvre, Polyhedral voronoi diagrams for additive manufacturing, ACM Transactions on Graphics (TOG) 37 (4) (2018) 1–15.
[9] T. Kuipers, J. Wu, C. C. Wang, Crossfill: foam structures with graded density for continuous material extrusion, Computer-Aided Design 114 (2019) 37–50.
[10] J. Martínez, M. Skouras, C. Schumacher, S. Hornus, S. Lefebvre, B. Thomaszewski, Star-shaped metrics for mechanical metamaterial design, ACM Transactions on Graphics (TOG) 38 (4) (2019) 1–13.
[11] S. G. Subramanian, M. Eng, V. R. Krishnamurthy, E. Akleman, Delaunay lofts: A biologically inspired approach for modeling space filling modular structures, Computers & Graphics 82 (2019) 73–83.
[12] E. Akleman, J. Chen, B. Meric, Web-based intuitive and effective design of symmetric tiles, Proceedings of ACM Multimedia 21 (4) (2000) 100–108.
[13] E. Akleman, V. R. Krishnamurthy, C.-A. Fu, S. G. Subramanian, M. Ebert, M. Eng, C. Starrett, H. Panchal, Generalized abeille tiles: Topologically interlocked space-filling shapes generated based on fabric symmetries, Computers & Graphics 89 (2020) 156–166.
[14] V. R. Krishnamurthy, E. Akleman, S. G. Subramanian, M. Ebert, J. Cui, C.-a. Fu, C. Starrett, Geometrically interlocking space-filling tiling based on fabric weaves, IEEE Transactions on Visualization & Computer Graphics 27 (01) (2021) 1–12.
[15] A. Molotnikov, Y. Estrin, A. V. Dyskin, E. Pasternak, A. Kanel-Belov, Percolation mechanism of failure of a planar assembly of interlocked osteomorphic elements, Engineering fracture mechanics 74 (8) (2007) 1222–1232.
[16] R. Lakes, Foam structures with a negative poisson's ratio, Science 235 (4792) (1987) 1038–1040.
[17] J. Wang, R. Rai, Generative design of conformal cubic periodic cellular structures using a surrogate model-based optimisation scheme, International Journal of Production Research (2020) 1–20.
[18] W. Xu, P. Zhang, M. Yu, L. Yang, W. Wang, L. Liu, Topology optimization via spatially-varying tpms, IEEE Transactions on Visualization and Computer Graphics.
[19] H. S. M. Coxeter, Twisted honeycombs, no. 4 in Conference Board on the Mathematical Sciences: Regional Conference Series in Mathematics, American Mathematical Society, 1970.
[20] H. S. M. Coxeter, Regular honeycombs in hyperbolic space, in: Proceedings of the International Congress of Mathematicians, Vol. 3, Citeseer, 1954, pp. 155–169.
[21] H. S. M. Coxeter, Regular polytopes, Courier Corporation, 1973.
[22] B. Grünbaum, G. C. Shephard, Tilings with congruent tiles, Bulletin of the American Mathematical Society 3 (3) (1980) 951–973.
[23] K. Sugihara, Voronoi-diagram approach to escher-like tiling, in: 2010 International Symposium on Voronoi Diagrams in Science and Engineering, IEEE, 2010, pp. 199–204.
[24] B. Grünbaum, G. C. Shephard, Tilings with congruent tiles, Bulletin of the American Mathematical Society 3 (3) (1980) 951–973.
[25] M. W. Schmitt, On space groups and dirichlet–voronoi stereohedra, Ph.D. thesis, Berlin: Freien Universität Berlin (2016).
[26] M. E. Rosa, M. Fortes, New types of space-filling polyhedra with fourteen faces, Acta Crystallographica Section A: Foundations of Crystallography 42 (4) (1986) 282–286.
[27] M. Goldberg, The space-filling pentahedra, Journal of Combinatorial Theory, Series A 13 (3) (1972) 437–443.
[28] M. Goldberg, The space-filling pentahedra. ii, Journal of Combinatorial Theory, Series A 17 (3) (1974) 375–378.
[29] M. Goldberg, Three infinite families of tetrahedral space-fillers, Journal of Combinatorial Theory, Series A 16 (3) (1974) 348–354.
[30] M. Goldberg, On the space-filling hexahedra, Geometriae Dedicata 6 (1) (1977) 99–108.
[31] M. Goldberg, On the space-filling heptahedra, Geometriae Dedicata 7 (2) (1978) 175–184.
[32] M. Goldberg, Convex polyhedral space-fillers of more than twelve faces, Geometriae Dedicata 8 (4) (1979) 491–500.
[33] M. Goldberg, On the space-filling octahedra, Geometriae Dedicata 10 (1-4) (1981) 323–335.
[34] M. Goldberg, On the space-filling enneahedra, Geometriae Dedicata 12 (3) (1982) 297–306.
[35] R. E. Williams, Space-filling polyhedron: its relation to aggregates of soap bubbles, plant cells, and metal crystallites, Science 161 (3838) (1968) 276–277.
[36] R. Williams, The geometrical foundation of natural structure: A source book of design, Dover New York, 1979.
[37] N. W. Johnson, Convex polyhedra with regular faces, Canadian Journal of Mathematics 18 (1966) 169–200.
[38] S. Alvarez, The gyrobifastigium, not an uncommon shape in chemistry, Coordination Chemistry Reviews 350 (2017) 3–13.
[39] H. S. M. Coxeter, Regular polytopes, Courier Corporation, 1973.
[40] M. Howison, C. H. Séquin, Cad tools for creating space-filing 3d escher tiles, Computer-Aided Design and Applications 6 (6) (2009) 737–748.
[41] H. Pottmann, M. Eigensatz, A. Vaxman, J. Wallner, Architectural geometry, Computers & graphics 47 (2015) 145–164.
[42] E. Akleman, J. Chen, Q. Xing, J. L. Gross, Cyclic plain-weaving on polygonal mesh surfaces with graph rotation systems, ACM Transactions on Graphics (TOG) 28 (3) (2009) 1–8.
[43] C. Jiang, J. Wang, J. Wallner, H. Pottmann, Freeform honeycomb structures, Computer Graphics Forum 33 (5) (2014) 185–194.
[44] C. Jiang, C. Tang, A. Vaxman, P. Wonka, H. Pottmann, Polyhedral patterns, ACM Trans. Graph. 34 (6). doi:10.1145/2816795.2818077.
URL https://doi.org/10.1145/2816795.2818077
[45] M. Meekes, A. Vaxman, Unconventional patterns on surfaces, ACM Trans. Graph. 40 (4). doi:10.1145/3450626.3459933.
URL https://doi.org/10.1145/3450626.3459933
[46] C. Schumacher, S. Marschner, M. Gross, B. Thomaszewski, Mechanical characterization of structured sheet materials, ACM Trans. Graph. 37 (4). doi:10.1145/3197517.3201278.
URL https://doi.org/10.1145/3197517.3201278
[47] C. Séquin, Intricate isohedral tilings of 3d euclidean space, in: Bridges Conference, Leeuwarden, The Netherlands, 2008, pp. 139–148.
[48] Z. Wang, P. Song, F. Isvoranu, M. Pauly, Design and structural optimization of topological interlocking assemblies, ACM Trans. Graph. 38 (6). doi:10.1145/3355089.3356489.
URL https://doi.org/10.1145/3355089.3356489
[49] E. Akleman, V. Krishnamurthy, C.-A. Fu, C. Starrett, S. G. Subramanian, D. Kim, N. Cropper, M. Ebert, Positive genus space-filling tiles, in: Proceedings of SMI'2021 Fabrication and Sculpting Event (FASE), 2021, pp. 65–68.
[50] B. N. Delaunay, N. N. Sandakova, Theory of stereohedra, Trudy Matematicheskogo Instituta imeni VA Steklova 64 (1961) 28–51.
[51] G. Voronoi, Nouvelles applications des paramètres continus à la théorie des formes quadratiques. deuxième mémoire. recherches sur les parallélloèdres primitifs., Journal für die reine und angewandte Mathematik (Crelles Journal) 1908 (134) (1908) 198–287.
[52] R. M. Erdahl, Zonotopes, dicings, and voronoi's conjecture on parallelohedra, European Journal of Combinatorics 20 (6) (1999) 527–549.
[53] A. Pugh, Polyhedra (Close-Packing Polyhedra), University of California Press, 2020.
[54] A. H. Schoen, On the graph (10,3)-a (2008).
[55] B. N. Delone, N. P. Dolbilin, S. Ryškov, M. Štogrin, A new construction in the theory of lattice coverings of an n-dimensional space by equal spheres, Mathematics of the USSR-Izvestiya 4 (2) (1970) 293.
[56] B. N. Delone, N. P. Dolbilin, M. I. Shtogrin, R. V. Galiulin, A local criterion for regularity of a system of points, Dokl. Akad. Nauk SSSR 227 (1) (1976) 19–21.
[57] J. C. Lagarias, Geometric models for quasicrystals i. delone sets of finite type, Discrete & Computational Geometry 21 (2) (1999) 161–191.
[58] J. C. Lagarias, Geometric models for quasicrystals ii. local rules under isometries, Discrete & Computational Geometry 21 (3) (1999) 345–372.
[59] J. C. Lagarias, P. A. Pleasants, Repetitive delone sets and quasicrystals, Ergodic Theory and Dynamical Systems 23 (3) (2003) 831–867.
[60] J. C. Lagarias, Meyer's concept of quasicrystal and quasiregular sets, Communications in mathematical physics 179 (2) (1996) 365–376.
[61] N. Dolbilin, Delone sets: local identity and global symmetry, in: Geometry and Symmetry Conference, Springer, 2015, pp. 109–125.
[62] N. Dolbilin, A. Garber, U. Leopold, E. Schulte, M. Senechal, On the regularity radius of delone sets in 3d, Discrete and Computational Geometry 66 (3) (2021) 996–1024.
[63] E. Fedorov, Symmetry on plane, in: Proc. Imperial Petersburg Mineralogical Soc., Vol. 28, 1891, pp. 345–390.

[64] T. Hahn, U. Shmueli, J. W. Arthur, International tables for crystallography, Vol. 1, Reidel Dordrecht, 1983.
[65] P. Barnes, J. K. Cockcroft, N. Deleeuw, A. L. Mackay, J. Bensted, R. E. G. and, A hypertext book of crystallographic space group diagrams and tables, http://img.chem.ucl.ac.uk/sgp/ (2024).
[66] H. Panchal, E. Akleman, V. Krishnamurthy, T. T. Yildiz, V. Grover, Curved space-filling tiles using voronoi decomposition with line, and curve segments closed under wallpaper symmetries (2023). `arXiv:2310.15361`.
[67] J. M. Montesinos-Amilibia, Classical tessellations and three-manifolds, Springer Science & Business Media, 2012.
[68] B. Grünbaum, What symmetry groups are present in the alhambra, Notices of the AMS 53 (6) (2006) 670–673.
[69] B. L. Bodner, et al., The planar crystallographic groups represented at the alhambra, Proc. Bridges 2013 (2013) 225–232.
[70] A. Bravais, Systems formed by points distributed regularly on a plane or in space, J. Ecole. Polytech. (1850) 1–128.
[71] A. Mois, U. Müller, H. Wondratschek, Historical introduction: International tables for crystallography (2006).
[72] L. Sohncke, Development of a theory of crystal structure, BG Teubner, 1879.
[73] E. S. von Fedorow, Compilation of the crystallographic results of mr. schoenflies and mine, Zeitschrift für Kristallographie-Crystalline Materials 20 (1-6) (1892) 25–75.
[74] A. M. Schoenflies, Remark on the article by mr. e. von fedorow, concerning the compilation of his crystallographic results and mine, Zeitschrift für Kristallographie-Crystalline Materials 20 (1-6) (1892) 259–262.
[75] P. Paufler, S. K. Filatov, Es fedorov promoting the russian-german scientific interrelationship, Minerals 10 (2) (2020) 181.
[76] M. Senechal, R. V. Galiulin, An introduction to the theory of figures: The geometry of es fedorov, Structural Topology 1984 núm 10.
[77] G. Polya, On the analogy of crystal symmetry in the plane, Zeitschrift für Kristallographie-Crystalline Materials 60 (1-6) (1924) 278–282.
[78] C.-V. Mauguin, On the symbolism of repetition or symmetry groups of crystalline assemblages, Zeitschrift für Kristallographie-Crystalline Materials 76 (1-6) (1931) 542–558.
[79] J. Conway, O. D. Friedrichs, D. H. Huson, W. P. Thurston, On three-dimensional space groups, arXiv preprint math/9911185.
[80] J. H. Conway, H. Burgiel, C. Goodman-Strauss, The symmetries of things, CRC Press, 2016.
[81] S. Ramsden, V. Robins, S. Hyde, Three-dimensional euclidean nets from two-dimensional hyperbolic tilings: kaleidoscopic examples, Acta Crystallographica Section A: Foundations of Crystallography 65 (2) (2009) 81–108.
[82] V. R. Krishnamurthy, E. Akleman, S. G. Subramanian, K. Boyd, C.-A. Fu, M. Ebert, C. Startett, N. Yadav, Bi-axial woven tiles: Interlocking space-filling shapes based on symmetries of bi-axial weaving patterns., in: Graphics interface, 2020, pp. 286–298.
[83] C. Mullins, M. Ebert, E. Akleman, V. Krishnamurthy, Voronoi spaghetti & voronoodles: Topologically interlocked, space-filling, corrugated & congruent tiles, in: SIGGRAPH Asia 2022 Technical Communications, ACM Siggraph, 2022, pp. 1–4.
[84] T. Yildiz, E. Akleman, V. Krishnamurthy, M. Ebert, A modular approach for creation of any bi-axial woven structure with congruent tiles, Computers & Graphics 114 (2023) 357–367.
[85] M. Ebert, E. Akleman, V. Krishnamurthy, R. Kulagin, Y. Estrin, Voronoodles: Topological interlocking with helical layered 2-honeycombs, Advanced Engineering Materials 26 (4) (2024) 2300831.
[86] A. V. Dyskin, Y. Estrin, E. Pasternak, H. C. Khor, A. J. Kanel-Belov, Fracture resistant structures based on topological interlocking with non-planar contacts, Advanced Engineering Materials 5 (3) (2003) 116–119.
[87] P. R. Cromwell, et al., Knots and links, Cambridge university press, 2004.
[88] A. Bicchi, V. Kumar, Robotic grasping and contact: A review, in: Proceedings 2000 ICRA. Millennium conference. IEEE international conference on robotics and automation. Symposia proceedings (Cat. No. 00CH37065), Vol. 1, IEEE, 2000, pp. 348–353.
[89] A. Dawari, D. Sen, Relation between part position and kinematic freedom: An expository survey, Mechanism and Machine Theory 45 (2) (2010) 157–169. `doi:https://doi.org/10.1016/j.mechmachtheory.2009.09.011`.
URL `https://www.sciencedirect.com/science/article/pii/S0094114X09001761`
[90] D. Austin, Fedorov's five parallelohedra, www.ams.org/publicoutreach/feature-column/fc-2013-11 (2022).
[91] Y. Nagai, A general framework for tilings, delone sets, functions, and measures and their interrelation, Discrete & Computational Geometry 62 (2) (2019) 241–291.

Appendix A. Discussion of Arrangement Operators and Properties of Their Compositions

Consider a cube C of unit length centered at $[0\ 0\ 0]^T \in \mathbb{R}^3$ and an arbitrary coordinate frame $F = \{\mathbf{\hat{n}_0}, \mathbf{\hat{n}_1}, \mathbf{\hat{n}_2}, \mathbf{O}\}$ *connected* to our unit cube C. Here, $\mathbf{\hat{n}_i}$ are linearly independent unit vectors and $\mathbf{O} = [x_O\ y_O\ z_O]^T \in \mathbb{R}^3$ is a vector whose tip represents that origin of F. Here, by "*connected to*", we mean that we apply symmetry operations induced by C to F. Without loss of generality, we assume that $\mathbf{O}$ lies inside C. Now, let us consider a rigid transformation $R(\mathbf{\hat{a}}, \theta)$ corresponding to rotation about an axis $\mathbf{\hat{a}}$ by an angle θ. The application of this transformation to F is defined as: $R(\mathbf{\hat{a}}, \theta)F := \{R(\mathbf{\hat{a}}, \theta)\mathbf{\hat{n}_0}, R(\mathbf{\hat{a}}, \theta)\mathbf{\hat{n}_1}, R(\mathbf{\hat{a}}, \theta)\mathbf{\hat{n}_2}, R(\mathbf{\hat{a}}, \theta)\mathbf{O}\}$

Based on the above, we define a *arrangement operator* $\mathcal{A} : F \mapsto \{F_i^*\}, i \in [0, n-1], n \in \mathbb{N}$ that takes a frame F as an input and produces a pattern F_i^* of *unique frames* through a combination of rotation and union (Figure 8). Specifically, we can define the following four *unit arrangement operators* $\mathcal{A}$ based on the isometries of the cube:

- **Vertex-centered Arrangement** ($\mathcal{V}_3$): Given a frame F and a given vertex-centered axis (i.e. a **b**ody diagonal) $\mathbf{\hat{b}_j}$, $j \in [0, 3]$, we have:
  $\mathcal{V}_3(j) : F \mapsto \{F_i^* = R(\mathbf{\hat{b}_j}, \frac{2i\pi}{3})F\}$ where $i \in [0, 2]$.
- **Edge-centered Arrangement** ($\mathcal{E}_2$): Given a frame F and a given **e**dge-centered axis $\mathbf{\hat{e}_j}$, $j \in [0, 5]$, we have:
  $\mathcal{E}_2(j) : F \mapsto \{F_i^* = R(\mathbf{\hat{e}_j}, i\pi)F\}$ where $i \in [0, 1]$.
- **Face-centered Arrangement** ($\mathcal{F}_2$): Given a frame F and a given **f**ace-centered axis $\mathbf{\hat{f}_j}$, $j \in [0, 2]$, we have:
  $\mathcal{F}_2(j) : F \mapsto \{F_i^* = R(\mathbf{\hat{f}_j}, i\pi)F\}$ where $i \in [0, 1]$.
- **Face-centered Arrangement** ($\mathcal{F}_4$): Given a frame F and a given **f**ace-centered axis $\mathbf{\hat{f}_j}$, $j \in [0, 2]$, we have:
  $\mathcal{F}_4(j) : F \mapsto \{F_i^* = R(\mathbf{\hat{f}_j}, \frac{i\pi}{2})F\}$ where $i \in [0, 3]$.

Observation 1

Here we note that the only requirement for two operators to be distinct is the axis of rotation. For example, for a given frame F, $\mathcal{V}_3(a)$ and $\mathcal{V}_3(b)$ $(a \neq b)$ generate two distinct patterns of F. The same applies to $\mathcal{E}_2$, $\mathcal{F}_2$, and $\mathcal{F}_4$.

Appendix A.1. Composition with Concatenation & Unique Copy Creation with Symmetry Operators

Given a frame F, a composition $\mathcal{A}_2 \circ \mathcal{A}_1$ is simply the application of $\mathcal{A}_2$ to all the frames generated by $\mathcal{A}_1$. Formally, if $\mathcal{A}_1 : F \mapsto \{F_i^*\}, i \in [0, n-1], n \in \mathbb{N}$ and $\mathcal{A}_2 : G \mapsto \{G_j^*\}, j \in [0, m-1], m \in \mathbb{N}$, then $\mathcal{A}_2 \circ \mathcal{A}_1 : F \mapsto \{F_k^*\}, k \in [0, mn-1]$.

Definition: Commutativity

Two operators $\mathcal{A}_1$, $\mathcal{A}_2$ are commutative if their compositions are order-independent. Specifically, the compositions $\mathcal{A}_1 \circ \mathcal{A}_2$ and $\mathcal{A}_2 \circ \mathcal{A}_1$ produce *identical arrangement up to a permutation*, i.e. the sets $(\mathcal{A}_1 \circ \mathcal{A}_2)(F)$ and $(\mathcal{A}_2 \circ \mathcal{A}_1)(F)$ are identical.

Observation 2

Compositions, in general, non-commutative, i.e. $\exists\ \mathcal{A}_1,\ \mathcal{A}_2$ such that $(\mathcal{A}_1 \circ \mathcal{A}_2)(F) \neq (\mathcal{A}_2 \circ \mathcal{A}_1)(F)$. This follows from the non-commutativity of matrix multiplication. However, as we will see later, commutativity turns out to be an important property for the design space of generalized Plesiohedra.

Observation 3

The total number of copies of F generated by a series of compositions $\mathcal{A}_q \circ \ldots \circ \mathcal{A}_1$ is the product $\prod_{i=1}^{q} n_i$ where n_i is the number of rotated copies of F generated by $\mathcal{A}_i$. However, the number of unique frames will always be less than or equal to $\prod_{i=1}^{q} n_i$.

Definition: Closure under $\mathcal{A}$

An arrangement $\mathcal{A}(F)$ is closed under $\mathcal{A}$ if all the produced frames are unique and non-repeating ($F^*_a \neq F^*_b$ iff $a \neq b$), and $(\mathcal{A} \circ \mathcal{A})(F)$ gives repeated copies of $\mathcal{A}(F)$. Alternately, $\mathcal{A}(F)$ is closed under $\mathcal{A}$ if $(\mathcal{A} \circ \mathcal{A})(F) = \mathcal{A}(F)$

Observation 4

It is easy to see that each unit operator ($\mathcal{V}_3(j)$, $\mathcal{E}_2(j)$, $\mathcal{F}_2(j)$, and $\mathcal{F}_4(j)$) produces an arrangement closed under itself. For example, $\mathcal{V}_3(j) \circ \mathcal{V}_3(j)$ will result in the same three copies of a given frame F.

Appendix A.2. Generalized Plesiohedral Tiling

The key requirement for a tiling to be Plesiohedral is that the Voronoi sites (typically points) form a symmetric Delone set. As a result, Voronoi tessellation of a set of sites arranged according to $\mathcal{A}$ will result in a tiling composed of a single unique prototile to fill the spaces. This follows from the general definition of Plesiohedral geometry that the Voronoi tessellation adopts the same symmetry as the underlying sites.

Without loss of generality, let us consider an arrangement of coordinate frames instead of points (we can always disregard the axes of the frames). Our central hypothesis is that if this frame arrangement is closed under a composition $\mathcal{A} := \mathcal{A}_q \circ \ldots \circ \mathcal{A}_1$ of arrangement operators, then repeating this arrangement in a cube grid will result in a symmetric Delone set. Since the arrangement was based on cube isometries, the set is automatically symmetric. The intuition behind the set being Delone is that the unique copy property ensures that the number of sites in the arrangement is maximal (applying the same operator will make no difference other than making copies). As a result, we posit that one can find an $\varepsilon > 0$ such that every two points of the set will be at least ε distance apart and every point in $\mathfrak{R}^3$ will be within a distance of $\frac{1}{\varepsilon}$ with at least one point in the set.

Although we do not formally prove this result here, we build our intuition by considering an example of an arrangement of frames repeated in a 2×2×2 grid. If we consider a secondary grid that is offset by half the length of the cube, we observe that the arrangement of sites in a unit cell of the secondary grid turns out to be some rigid transformation of the original arrangement up to flipping of the coordinate axes of the frames. What this implies is that the distance relationships between the individual elements (frames) of an arrangement within a unit cell is maintained even between the elements of the neighboring cells.

Our key extension, however, is that the Voronoi sites are allowed to be higher-dimensional, i.e. they can be lines, curves, curve complexes, surfaces, etc. Specifically, the idea is to ***sample points*** on higher-dimensional sites to approximate the sites in a piecewise linear manner. What this implies is that any rigid transformation applied to a higher-dimensional site (which, in itself, can be a continuous and even smooth geometric object) is effectively applied to a discrete set of points associated with (i.e. sampled from) it. This discretized interpretation of higher-dimensional sites allows for the direct application of symmetric Delone property which is otherwise only relevant to point sets. The intuition behind this comes from the recent works by Dolbilin [61, 62] and Nagai [91]. We observe that since generalized Plesiohedra are produced by a set of points sampled on some skeletal shape, the Voronoi sites are ultimately the points, each point still produces a convex polyhedron as its Voronoi region. However, it is their union that appears curved. Therefore, a generalized Plesiohedra is still a polyhedron with a high number of flat faces and straight edges that can be non-convex and positive genus unlike a standard Plesiohedra. In conjunction, these two observations lead to a rich design space for generalized Plesiohedra.

Appendix A.3. Enumerating the Arrangement Design Space

The final step in our conceptual framework is to enumerate, classify, and characterize the compositions of operators that lead to a symmetric Delone set. This is essential to enumerate the design space of the arrangement of the Voronoi sites (whatever shape they may take). We note that because the arrangement operator creates rotated copies of an input object based on the isometries of the cube, there will always be *a finite maximum number of unique non-repeating copies* of a given frame (or any rigid object) that can be generated. In other words, if we apply an arbitrarily long composition, say $\mathcal{A} := \mathcal{A}_q \circ \ldots \circ \mathcal{A}_1$ to a frame F, the set $\{F^*_i\}$ will be a finite set with the maximum possible value for i such that $F^*_a \neq F^*_b$ if $a \neq b$. Furthermore, we want the set $\{F^*_i\}$ to close under $\mathcal{A}$.

As an example, consider a composition of two arrangement operators, say, $\mathcal{E}_2(1) \circ \mathcal{V}_3(0)$. We get six unique matrices based on the Cartesian products of the sets $\{R(\hat{\mathbf{e}}_1, 0), R(\hat{\mathbf{e}}_1, \pi)\}$ and $\{R(\hat{\mathbf{b}}_0, 0),\ R(\hat{\mathbf{b}}_0, \frac{2\pi}{3}), R(\hat{\mathbf{b}}_0, \frac{4\pi}{3})\}$. As a result, we get six unique non-repeating copies of the frame F (Figure A.22(a)). Note that the composition can also be done between two operators of the same type but about different axes. For example, $\mathcal{E}_2(1) \circ \mathcal{E}_2(0)$ results in four unique non-repeating copies of the frame F (Figure A.22(c)). Specifically, we investigate the following questions in this regard:

1. How are closure and commutativity related? Does one result in the other?

2. What is the maximum number of non-repeating (unique) copies of F that can be generated through a composition of arrangement operators?

3. What is the minimum number q such that $(\mathcal{A}_q \circ \ldots \circ \mathcal{A}_1)(F)$ enumerates all possible non-repeating (unique) copies of F?

In order for the completeness of this work, we follow an experimental strategy for enumeration of all combinations of operators

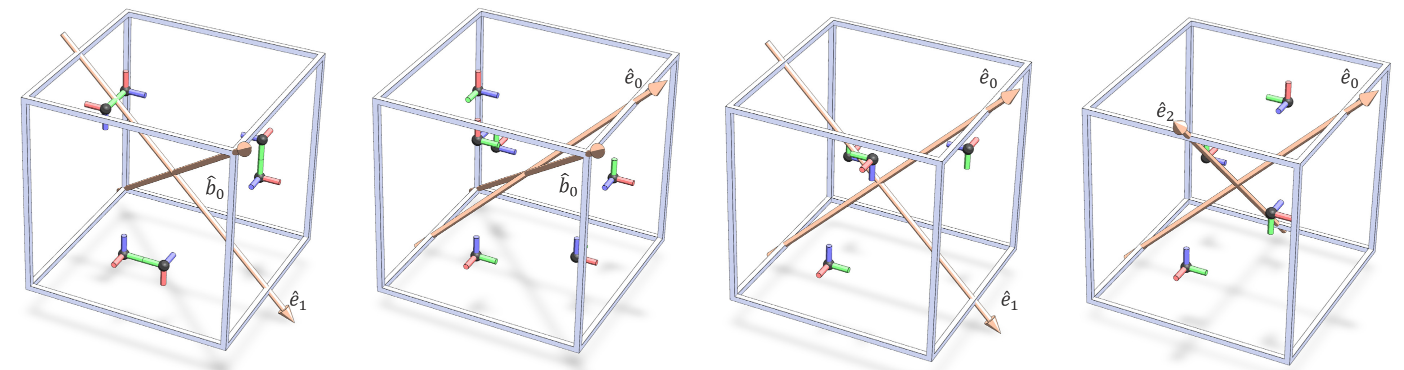

(a) Composition of two operators, $\mathcal{E}_2(1) \circ \mathcal{V}_3(0)$

(b) Composition of two operators, $\mathcal{E}_2(0) \circ \mathcal{V}_3(0)$

(c) Composition of two operators, $\mathcal{E}_2(0) \circ \mathcal{E}_2(1)$

(d) Composition of two operators, $\mathcal{E}_2(0) \circ \mathcal{E}_2\ (2)$

Figure A.22: Four examples shown using various different operators. Only (a) and (c) are closed under their operators, while (b) and (d) are not closed under their operation, and any repetition of these operations would result in additional sites created.

.

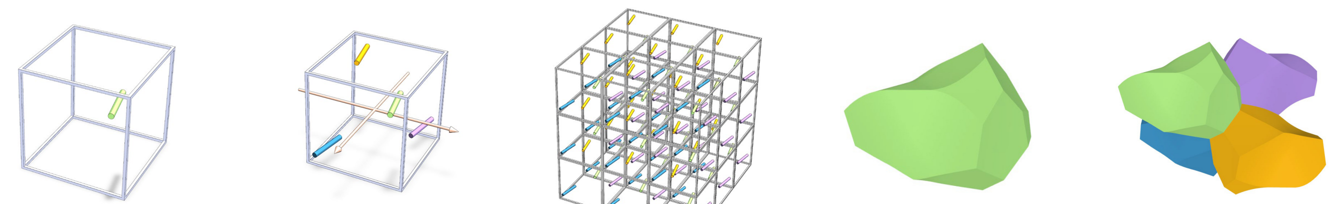

(a) Single line chosen

(b) Arrangement operator applied

(c) Patterned

(d) Single unit tile

(e) Combination of Unit Tiles

Figure A.23: The general methodology of our process is shown where a single curve is chosen (a) and the arrangement operator is then applied (b). This can then be patterned (c) and finally the Voronoi decomposition is taken, which results in a unit tile (d). The unit tile is repeated and can be shown in a combination (e).

up to 3 operators. The entire list of which operators are closed under other operators is described in detail in the appendix. In this work, we only choose to use operators which are closed and therefore create identical plesiohedron.

We wish to emphasize that while closely related to each other, the notions of closure and the creation of unique copies are not identical. In creating unique copies, our goal is to create all (sufficient) and only (necessary) copies of the set that can form the Delone set. To obtain these, we use the closure property already inherent in cystallographic symmetry groups. However, the key idea is to use the combination of symmetry **operations** in such a way that we can create all unique copies and only unique copies without any repetition. This is equivalent to identifying all unique matrices that are obtained by concatenating the matrices that correspond to all symmetry operations of a given symmetry group that gives closure. We, therefore, look at multi-operator compositions.

Appendix A.4. Two-operator compositions for Unique Copy Generation

All two-operator compositions are shown below.

1. $\mathcal{F}_4 \circ \mathcal{V}_3$, $\mathcal{F}_2 \circ \mathcal{V}_3$, $\mathcal{V}_3 \circ \mathcal{F}_4$, and $\mathcal{V}_3 \circ \mathcal{F}_4$: All of these operators are not closed and no combination will lead to them being closed.

2. $\mathcal{F}_4 \circ \mathcal{E}_2$, $\mathcal{F}_2 \circ \mathcal{E}_2$, $\mathcal{E}_2 \circ \mathcal{F}_4$, and $\mathcal{E}_2 \circ \mathcal{F}_2$: Given an edge it will be closed for the face vector that has a component that is not on that edge. For example the operator $\mathcal{E}_2(0)$ will be closed with a face operator of $\mathcal{F}_4(2)$ but not if the face operator is $\mathcal{F}_4(0)$.

3. $\mathcal{V}_3 \circ \mathcal{E}_2$, $\mathcal{E}_2 \circ \mathcal{V}_3$: If the edge on which $\mathcal{E}_2$ lies does not contain a vertex on which $\mathcal{V}_3$ passes through, then the shape will be closed. Ex: Given the operator $\mathcal{V}_3(2)$ the following operators will result in a closed operation $\mathcal{E}_2(0)$, $\mathcal{E}_2(4)$, and $\mathcal{E}_2(3)$.

4. $\mathcal{V}_3 \circ \mathcal{V}_3$: Only two operations around the same axis will result in a closed operation.

5. $\mathcal{E}_2 \circ \mathcal{E}_2$: There are two times in which the operation will be closed, if the operators are around the same axis, as well as if a plane connecting the two axis is a mid-plane of the cube, where a mid-plane is a plane parallel to two opposite faces and passes through the center of the cube.

6. $\mathcal{F}_2 \circ \mathcal{F}_2$: The two operations will always be closed no matter the order or axis.

7. $\mathcal{F}_4 \circ \mathcal{F}_4$: The two operations will only be closed when they operate on the same axis.

From this enumeration of the space we notice several things, the first being that every combination that is closed is also commutative. This is seen in Figure A.25 because the matrix is fully symmetric along its diagonal. Second, there are some combinations of operators that will always be closed $\mathcal{F}_2 \circ \mathcal{F}_2$ and some that will never be closed $\mathcal{F}_4 \circ \mathcal{V}_3$ and $\mathcal{F}_2 \circ \mathcal{V}_3$.

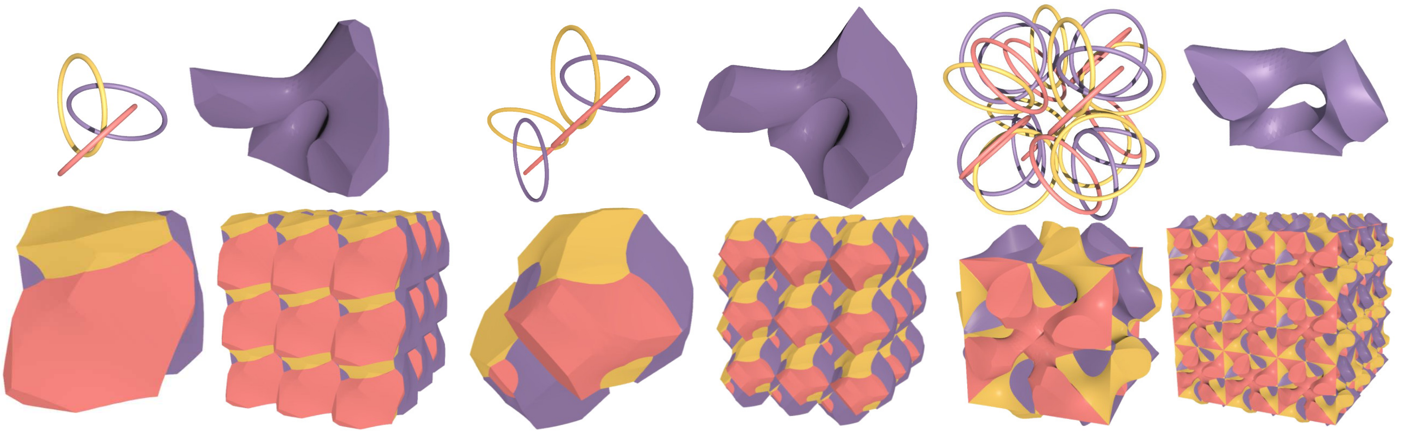

(a) $\mathcal{V}_3(0)$ (b) $\mathcal{E}_2(1) \circ \mathcal{V}_3(0)$ (c) $\mathcal{F}_4(2) \circ \mathcal{E}_2(1) \circ \mathcal{V}_3(0)$

Figure A.24: A step by step approach of multiple operators. Starting with $\mathcal{V}_3(0)$ operator (a) with the resulting unit tile, 3 tile assembly and larger assembly. Then $\mathcal{E}_2(1) \circ \mathcal{V}_3(0)$, and finally the operators $\mathcal{F}_4(2) \circ \mathcal{E}_2(1) \circ \mathcal{V}_3(0)$

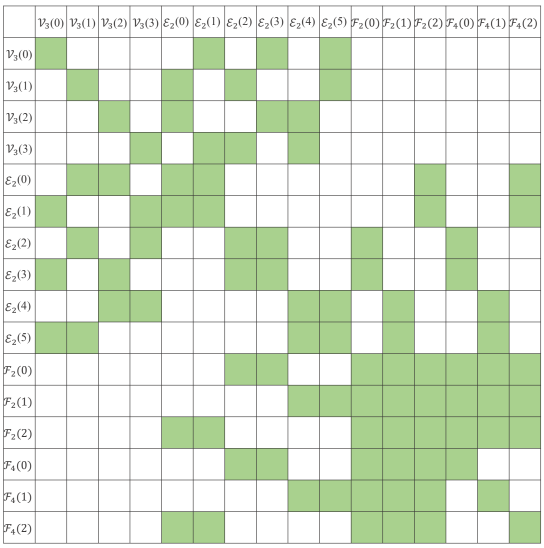

Figure A.25: A matrix of all possible combinations of two operators. Each green square represents those two corresponding operations being closed. The matrix is symmetric about its diagonal which means that for two operators it is order independent.

Appendix A.5. Three-operator compositions for Unique Copy Generation

When looking at three successive operators, there is one unique characteristic, when three operators are closed, it can only have 8, 12, or 24 total unique frames after patterning. These numbers of unique frames are what we study to determine closure. One note is that the three operations are symmetric around the middle operator, which means that $\mathcal{E}_2(i) \circ \mathcal{F}_4(j) \circ \mathcal{V}_3(k)$ is equivalent to $\mathcal{V}_3(i) \circ \mathcal{F}_4(j) \circ \mathcal{E}_2(k)$.

1. 8 Sites: The only way to get 8 sites is when the only three operators are $\mathcal{F}_2$ or $\mathcal{E}_2$ because they double the number of sites each time which after three operations results in 8 sites. The only time when this operation is closed is through the following.
   (a) $\mathcal{F}_2(i) \circ \mathcal{E}_2(j) \circ \mathcal{E}_2(k)$: Where $\mathcal{F}_2(i) \circ \mathcal{E}_2(j)$ is not closed.
   (b) $\mathcal{F}_2(i) \circ \mathcal{E}_2(j) \circ \mathcal{F}_2(k)$: Where $i \neq k$.
   (c) $\mathcal{F}_2(i) \circ \mathcal{F}_2(j) \circ \mathcal{E}_2(k)$: Where $i \neq j$
2. 12 Sites: The process to obtain a closed 12 sites only contains $\mathcal{F}_2$ and $\mathcal{V}_3$ as the operators. The only process to obtain a closed 12 site symmetry is the following
   (a) $\mathcal{F}_2(i) \circ \mathcal{F}_2(j) \circ \mathcal{V}_3(k)$: Where $i \neq j$
3. 24 Sites: The maximum number of unique sites that can be obtained is 24. This happens only when the operations include $\mathcal{F}_4$, $\mathcal{V}_3$, and $\mathcal{E}_2$ or $\mathcal{F}_2$. The following conditions are when all 24 sites occur.
   (a) $\mathcal{F}_4(i) \circ \mathcal{V}_3(j) \circ \mathcal{E}_2(k)$: Where $\mathcal{V}_3(j) \circ \mathcal{E}_2(k)$ is closed in the two operator case.
   (b) $\mathcal{V}_3(i) \circ \mathcal{E}_2(j) \circ \mathcal{F}_4(k)$: Where $\mathcal{F}_4(i) \circ \mathcal{E}_2(j)$ or $\mathcal{E}_2(j) \circ \mathcal{V}_3(k)$ is closed in the two operator case.
   (c) $\mathcal{F}_4(i) \circ \mathcal{F}_2(j) \circ \mathcal{V}_3(k)$: Where $i \neq j$.
   (d) $\mathcal{E}_2(i) \circ \mathcal{F}_4(j) \circ \mathcal{V}_3(k)$: Where $\mathcal{E}_2(i) \circ \mathcal{F}_4(j)$ is closed in the two operator case.
   (e) $\mathcal{F}_2(i) \circ \mathcal{F}_4(j) \circ \mathcal{V}_3(k)$: Where $i \neq j$.

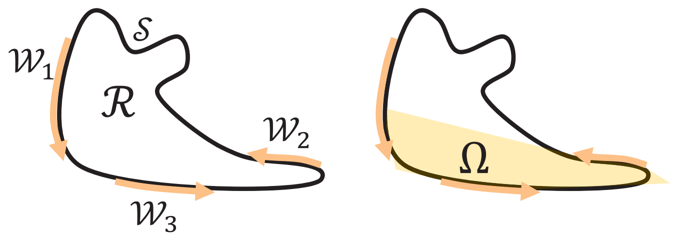

(a) A region with walls that has a bounded feasible space (DoF = 0)

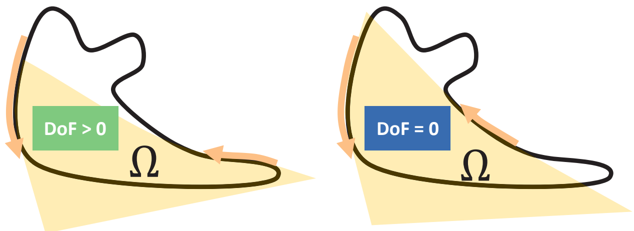

(b) Feasible spaces are unbounded in both cases

Figure B.26: Problem definition for kinematic constraint analysis for an object in contact with walls. The walls are modeled as portions of the surface of the object as in the case of space-filling structures.

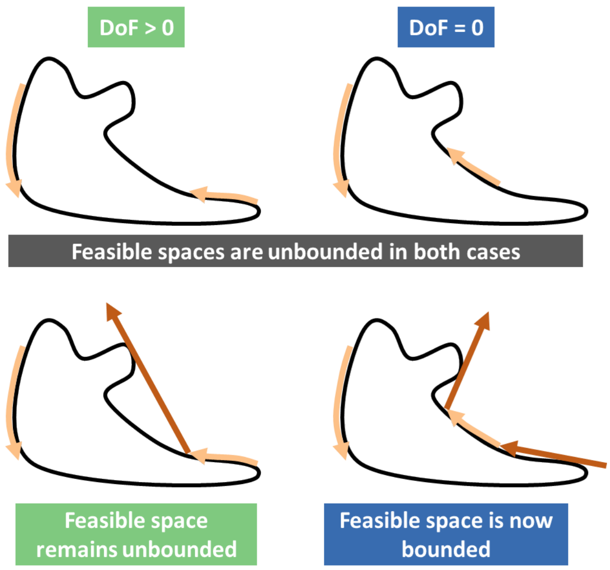

Figure B.27: Our approach to resolving the ambiguity for unbounded feasible regions is illustrated.

We note here that a maximal arrangement of sites for cube isometries contains 24 unique copies of a site. Given that this can be achieved by three compositions, any subsequent composition of operators does not result in a closed arrangement. Therefore, all one-, two-, and three-operator arrangements enumerate the complete set of arrangements possible (Figure A.24).

Appendix B. Methodology for Interlocking Analysis

Here we provide a formal description of the algorithm we implemented for our analytical study (Section 5). Our problem to determine whether a central tile is immovable ($DoF = 0$) or movable ($DoF > 0$) under the kinematic constraints imposed by its neighboring tiles. In the most general form, consider a volume of space $\mathcal{R}$ space bounded by a closed orientable surface $\mathcal{S}$. Let $\mathcal{W}_i$ be surface patches on $\mathcal{S}$ that represent a set of *fixed walls* that restrict $\mathcal{R}$ to translate. The question is whether $DoF(\mathcal{R}) = 0$ or not. Given this problem, we make the following assumptions for our analysis:

- $\mathcal{R}$ has no holes. In other words, it is genus-0 solid.
- $\mathcal{R}$ has no rotational degrees of freedom, i.e. we are considering only ***translational*** degrees of freedom.
- $\mathcal{S}$ is allowed to be smooth, piece-wise linear, or a combination of smooth and linear patches. $\mathcal{S}$ does not contain any spherical patches.
- $\mathcal{S}$ is represented as an orientable surface (or piece-wise linear approximation in the discrete case).
- All contacts between $\mathcal{S}$ and are $\mathcal{W}_i$ are surface contacts.
- All $\mathcal{W}_i$ are open surfaces.

Appendix B.1. Problem & Approach in the Continuous Case

Under the given assumptions, the key idea behind our algorithm is that a set of walls on an object defines a feasibility region $\Omega(\mathcal{S}, \{\mathcal{W}_i\})$ (Figure B.26(a)). The feasibility region Ω_i a wall $\mathcal{W}_i$ is defined as the intersection of all the half-spaces of all tangents of $\mathcal{W}_i$. Therefore, the total feasibility region is defined as i.e. $\Omega(\mathcal{S}, \{\mathcal{W}_i\}) := \bigcap \lim_{i=1}^{n} \Omega_i$. Note that Ω is always convex.

If $\Omega(\mathcal{S}, \{\mathcal{W}_i\})$ is bounded, then the object is immovable under translation regardless of whether the object is convex or not (Figure B.26(a)). However, for non-convex objects, an unbounded feasibility region results in an ambiguous case wherein the geometry of the walls in relation to the shape of the object affect the decision regarding the object's mobility (Figure B.26(b)). We resolve this ambiguity using an interesting observation related to the convex hull of the object. The basic idea is that the location of a wall on the concave segments of a boundary results in an unbounded feasibility region leading to ambiguity. Therefore, we construct additional walls to resolve the ambiguity. In other words, we wish to add walls such that the additional constraints imposed by those walls do not alter the DoF unless the object it was originally 0. To do this, our strategy is simple. For each concave wall, we must determine the largest region bounded by two rays that: (1) have one end at the end-point of the wall and (2) are tangent to the boundary curve at some point (Figure B.27).

Appendix B.2. Algebraic Formulation in Discrete Setting

In the discrete case, $\mathcal{S}(V, F)$ is a polygonal mesh with a set of vertices V and an indexed face-list $F = \{f_i\}$, $i \in [0, n+m-1]$. Assume that all faces in F are planar and are represented as $f_i := (\mathbf{\hat{n}_i}, \mathbf{c_i})$, where $\mathbf{\hat{n}_i}$ is the face normal in the outward direction and $\mathbf{c_i}$ is the center of the face. We consider two mutually exclusive and exhaustive subsets $W,\ U \subset F \mid U \cup W = F,\ U \cap W = \emptyset$. Here, $W = \{w_j = (\mathbf{\hat{n}_j^W}, \mathbf{c_j^W})\}$, $j \in [0, n-1]$ is a set of faces that represent the walls and $U = \{u_k = (\mathbf{\hat{n}_k^U}, \mathbf{c_k^U})\}$, $k \in [0, m-1]$ are the set of unrestricted faces. Based on these sets, we pose our problem as a linear program of the form:

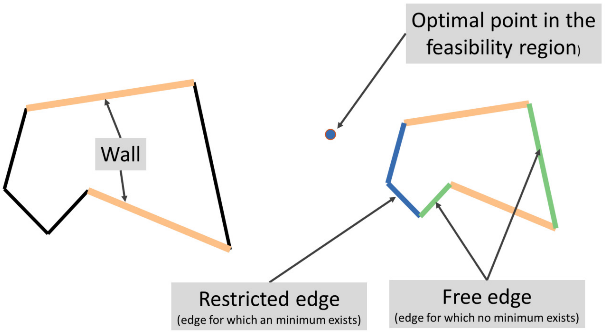

(a) Nomenclature (color-coding) for walls and unrestricted edges.

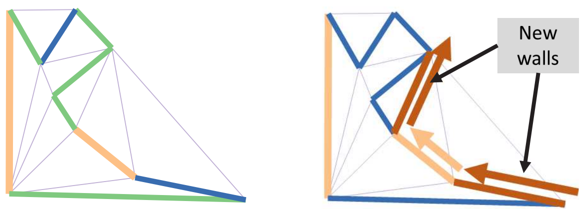

(b) Addition of new walls based on Delaunay triangulation.

Figure B.28: The algorithm for computing additional walls based on the Delaunay triangulation is shown.

$$\begin{aligned} &\text{Given: } \gamma_k \in \mathbb{R}^3 \ (k \in [0, m-1]) \\ &\text{find: } \mathbf{x} \in \mathbb{R}^3 \text{ that minimizes: } \gamma_j^T \mathbf{x} \\ &\text{under the constraints: } A\mathbf{x} \leq \beta \end{aligned} \qquad \text{(B.1)}$$

Here, $\gamma_k^T \mathbf{x}$ is the objective function for an unrestricted face u_k and $\mathbb{R}^{n \times 3} \ni \gamma_k = -\hat{\mathbf{n}}_{\mathbf{k}}^{\mathbf{U}}$ represents the ***inward normal*** of the face $u_k \in U$. The constraints (A and β) are given by:

$$\mathbb{R}^{n\times 3} \ni A = \begin{bmatrix} (\hat{\mathbf{n}}_{\mathbf{0}}^{\mathbf{W}})^T \\ (\hat{\mathbf{n}}_{\mathbf{1}}^{\mathbf{W}})^T \\ \vdots \\ (\hat{\mathbf{n}}_{\mathbf{n-1}}^{\mathbf{W}})^T \end{bmatrix} \qquad \text{(B.2)}$$

$$\mathbb{R}^{3\times 1} \ni \beta = \begin{bmatrix} (\hat{\mathbf{n}}_{\mathbf{0}}^{\mathbf{W}})^T \mathbf{c}_{\mathbf{0}}^{\mathbf{W}} \\ (\hat{\mathbf{n}}_{\mathbf{1}}^{\mathbf{W}})^T \mathbf{c}_{\mathbf{1}}^{\mathbf{W}} \\ \vdots \\ (\hat{\mathbf{n}}_{\mathbf{n-1}}^{\mathbf{W}})^T \mathbf{c}_{\mathbf{n-1}}^{\mathbf{W}} \end{bmatrix} \qquad \text{(B.3)}$$

In terms of physical interpretation, our constraint inequality essentially models each face w_j as a wall such that the object can move only ***in the direction of the inward normal***. Therefore, our approach is essentially to consider each unrestricted face u_k and ask the question: "*if u_k is only allowed to move **in the direction defined by its positive normal**, is there an optimum solution for u_k in the feasibility region defined by the constraints?*". Note that to allow u_k to move in the direction of its positive normal, the coefficient vector γ_k of the corresponding objective should be opposite to the outward normal for a minimization problem.

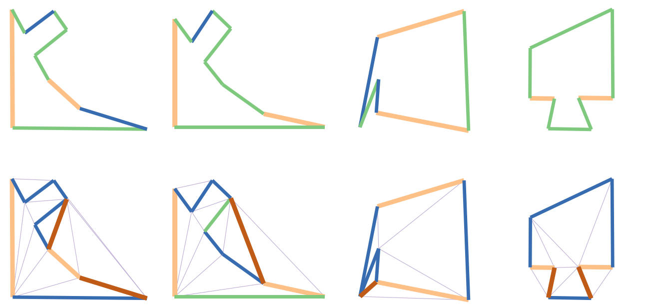

(a) DoF = 0 (b) DoF > 0 (c) DoF = 0 (d) DoF = 0

Figure B.29: Explanatory results are shown for DoF analysis for a set of 2D polygonal shapes. The top rows display the result of the linear program before the addition of new walls and the bottom row shows the final result. These images were generated by the 2D version of our algorithm.

Appendix B.3. Algorithm

Based on the physical interpretation, there are three possibilities for each unrestricted face. First, the face may have an optimum in the feasibility region. Second, the face may be able to more freely within the feasibility region, i.e. the optimal solution is infinite (unbounded). Third, there is no optimal solution for the face within the feasibility region. In order for the entire shape to be immovable ($Dof = 0$), either each unrestricted face should have an optimum in the feasibility region (i.e. it will be restricted by some vertex of the feasibility region) or there should be no optimal solution within the feasibility region (i.e. the region of allowable motion of the face does not intersect with the feasibility region defined by the walls). Based on this observation our algorithm (Figure B.28) is as follows:

Input: $A, \beta, U = \{u_k = (\hat{\mathbf{n}}_{\mathbf{k}}^{\mathbf{U}}, \mathbf{c}_{\mathbf{k}}^{\mathbf{U}})\},\ k \in [0, m-1]$

Output: **boolean** $isMovable$

integer $Count \leftarrow 0$

For each $k \in [0, m-1]$

$\gamma_k \leftarrow -\hat{\mathbf{n}}_{\mathbf{k}}^{\mathbf{U}}$

$[\mathbf{x}, flag] \leftarrow LinearProgram(\gamma_k^T, A, \beta)$

If ($flag$ = 'Optimal Solution-Exists')

$Count \leftarrow Count + 1$

End If

If $Count = m$

$isMovable \leftarrow false$

Else

$DT \leftarrow Delaunay(\mathcal{S})$

$HULL \leftarrow ConvHull(\mathcal{S})$

For each $j \in [0, n-1]$

Add the face at the boundaries of w_j not on the convex hull as a new wall. Update A and β

Repeat linear program with updated A and β

If all faces in U admit optimal solution

$isMovable \leftarrow false$

Else

```
            isMovable ← false
        End If
    End If
Return isMovable
```

We conducted a preliminary analysis of our algorithm in 2D for polygonal shapes to evaluate its correctness. Our method using the linear programming approach was able to successfully classify each case (Figure B.29).